CANCER COMMUNICATIONS
Open Access

ORIGINAL ARTICLE

Leptin-mediated suppression of lipoprotein lipase cleavage enhances lipid uptake and facilitates lymph node metastasis in gastric cancer

Jian Xiao | Shuqing Cao | Jiawei Wang | Pengyu Li | Quan Cheng | Xinyi Zhou | Jiacheng Dong | Yuan Li | Xinyu Zhao | Zekuan Xu | Li Yang 🔟

Department of General Surgery, The First Affiliated Hospital of Nanjing Medical University, Nanjing, Jiangsu, P. R. China

Correspondence
Li Yang, Department of General Surgery, The First Affiliated Hospital of Nanjing Medical University, 300 Guangzhou Road, Nanjing 210029, Jiangsu, P. R. China.
Email: pwkyangli@njmu.edu.cn

Abstract

Background: Lymph node metastasis (LNM) is the primary mode of metastasis in gastric cancer (GC). However, the precise mechanisms underlying this process remain elusive. Tumor cells necessitate lipid metabolic reprogramming to facilitate metastasis, yet the role of lipoprotein lipase (LPL), a pivotal enzyme involved in exogenous lipid uptake, remains uncertain in tumor metastasis. Therefore, the aim of this study was to investigate the presence of lipid metabolic reprogramming during LNM of GC as well as the role of LPL in this process.

Methods: Intracellular lipid levels were quantified using oil red O staining, BODIPY 493/503 staining, and flow cytometry. Lipidomics analysis was employed to identify alterations in intracellular lipid composition following LPL knockdown. Protein expression levels were assessed through immunohistochemistry, Western blotting, and enzyme-linked immunosorbent assays. The mouse popliteal LNM model was utilized to investigate differences in LNM. Immunoprecipitation and mass spectrometry were employed to examine protein associations. In vitro phosphorylation assays and Phos-tag sodium dodecyl-sulfate polyacrylamide gel electrophoresis assays were conducted to detect angiopoietin-like protein 4 (ANGPTL4) phosphorylation.

- -

Results: We identified that an elevated intracellular lipid level represents a crucial characteristic of node-positive (N+) GC and further demonstrated that a high-fat diet can expedite LNM. LPL was found to be significantly overexpressed in N+ GC tissues and shown to facilitate LNM by mediating dietary lipid uptake within GC cells. Leptin, an obesity-related hormone, intercepted the effect exerted by ANGPTL4/Furin on LPL cleavage. Circulating leptin binding to the leptin receptor could induce the activation of inositol-requiring enzyme-1 (IRE1) kinase, leading to the phosphorylation of ANGPTL4 at the serine 30 residue and subsequently reducing its binding affinity with LPL. Moreover, our research revealed that LPL disrupted lipid homeostasis by elevating intracellular levels of arachidonic acid, which then triggered the cyclooxygenase-2/prostaglandin E2 (PGE2) pathway, thereby promoting tumor lymphangiogenesis.

Conclusions: Leptin-induced phosphorylation of ANGPTL4 facilitates LPL-mediated lipid uptake and consequently stimulates the production of PGE2, ultimately facilitating LNM in GC.

KEYWORDS
angiopoietin-like protein 4, leptin, lipoprotein lipase, lymph node metastasis, prostaglandin E2

1 | BACKGROUND

Gastric cancer (GC) is one of the most prevalent malignant neoplasms affecting the digestive tract, ranking fifth globally in terms of incidence and fourth in mortality [1]. In China, GC holds the third position among all malignancies regarding both incidence and mortality rates [2, 3]. It is estimated that between 2021 and 2035, approximately 5.6 million individuals will succumb to GC in China [4]. Lymph node metastasis (LNM) represents the predominant mode of dissemination for GC cells [5]. The presence of LNM signifies enhanced invasiveness and distant metastatic potential, indicating an unfavorable prognosis with a heightened risk of recurrence [6]. Furthermore, LNM bears significant clinical implications for early-stage GC patients as it serves as a crucial determinant when formulating treatment strategies [5]. Significantly, despite the substantial advancements in systematic treatment of GC, the prognosis for GC patients continues to be significantly hindered by the metastasis of the disease [7–10]. Therefore, investigating the mechanisms underlying LNM in GC assumes paramount importance.

In recent years, numerous studies have demonstrated that cancer cells undergo lipid metabolism reprogramming during metastasis to meet the escalating demand for lipids [11–13]. Lee *et al.* [14] reported that metastatic cancer cells can promote LNM through metabolic reprogramming towards fatty acid β-oxidation. Other studies have suggested lipid metabolites, such as prostaglandin E2 (PGE2), may stimulate tumor lymphangiogenesis [15, 16]. We previously reported the positive association between body mass index (BMI) and LNM, indicating a crucial role of dysregulated lipid metabolism in promoting LNM in GC [17]. The ways for cancers to obtain lipids include endogenous synthesis and exogenous uptake [18]. Studies have shown that cancer cells can acquire lipids by de novo lipogenesis [19, 20]. Although dietary sources of lipids are another way, whether GC cells acquire dietary lipids remains unclear. Previous studies have shown that a high-fat diet (HFD) can increase intracellular lipid levels in GC cells [21, 22]. Kitayama *et al.* [23] found that hypertriglyceridemia was an independent risk factor for LNM in early male GC. Therefore, an exogenous supply of lipids for GC cells may exert a significant effect on the LNM of GC.

Lipoprotein lipase (LPL) is a crucial secreted enzyme for serum lipid uptake that can hydrolyze triglycerides in chylomicron or very low-density lipoproteins (VLDLs) on the surface of the capillary lumen to produce free fatty acids [24, 25]. In addition, LPL can facilitate the endocytosis of lipoproteins in a non-enzymatic manner [26]. Previous studies showed that LPL is involved in the lipid uptake of cancers to promote cell proliferation [27, 28]. However, the role of LPL in GC has not been reported yet. Of note, the expression and enzymatic activity of LPL are tightly regulated by a variety of mechanisms in response to the metabolic state and energy requirements of cells. Angiopoietin-like protein 4 (ANGPTL4) is the main factor that post-translationally inactivates LPL through

various approaches, such as enhancing the cleavage of LPL by the proprotein cleavage enzyme Furin or irreversibly promoting the unfolding of the domain of LPL monomer hydrolase [29]. Hence, for tumor cells, disrupting the negative regulation of ANGPTL4 on LPL is of great significance.

The enhanced uptake of exogenous lipids by cancer cells has led to the recognition that LPL may be an important component of the interaction between dietary lipids and cancer biology. This study aimed to investigate potential differences in lipid accumulation levels between node-positive and node-negative primary GC tissues, as well as explore the impact of LPL-mediated exogenous lipid uptake on the LNM of GC. Additionally, we further delved into the molecular mechanism underlying the abnormal activation of LPL in GC cells and examined how LPL-induced alterations in lipid metabolism contribute to changes in the metastatic pattern of GC cells.

2 | MATERIALS AND METHODS

2.1 | Tissue samples and cell lines

Tumor and adjacent normal tissues were collected from 57 GC patients who underwent gastrectomy at the First Affiliated Hospital of Nanjing Medical University (Nanjing, Jiangsu, China). Histological assessment revealed that among the 57 GC samples, 22 were lymph node-negative (N0), while 35 were lymph node-positive (N+). All patients had not received any treatment before surgery. The collected tissue samples were promptly frozen in liquid nitrogen and stored at -80°C until further use. The frozen tissue sections were immediately stained with oil red O dye. This study was ethically approved by the Ethics Committee of the First Affiliated Hospital of Nanjing Medical University, and written informed consent was obtained from all participants before specimen collection.

For this study, we utilized 6 GC cell lines (MKN45, HGC27, AGS, MKN28, NCI-N87, and SNU-719) and a normal human gastric mucous epithelium cell line (GES-1). MKN45, HGC27, AGS, and GES-1 were obtained from the Cell Bank of the Chinese Academy of Science (Shanghai, China). MKN28, NCI-N87, and SNU-719 were purchased from the American Type Culture Collection (ATCC, Manassas, VA, USA). Human lymphatic endothelial cells (HLECs) were obtained from ScienCell Research Laboratories (San Diego, CA, USA). GES-1, HGC27, MKN28, MKN45, NCI-N87, and SNU-719 were cultured in the RPMI-1640 medium (Wisent, Montreal, Canada), while the AGS cell line was cultured in the F12K medium (Wisent). All media were supplemented with 10% fetal bovine serum (FBS; Wisent)

and 1% penicillin/streptomycin (Wisent). The low-glucose medium was prepared from standard medium to sugar-free medium in a 1:2 ratio (Gibco, Grand Island, NY, USA). HLECs were cultured in an endothelial cell medium with 5% FBS. All cells were maintained in a humidified incubator with 5% CO_2 at 37°C.

2.2 | Plasmids, small interfering RNAs (siRNAs), short hairpin RNA (shRNA), and cell transfection

siRNA oligonucleotides targeting *LPL*, *ANGPTL4*, leptin receptor (*LEPR*), and cyclooxygenase-2 (*COX2*), as well as negative control siRNA, were purchased from GenePharma (Shanghai, China). The full-length *LPL* or shRNA sequences that targeted *LPL* were subcloned and amplified into lentiviral expression vectors (GenePharma, Shanghai, China) to establish stable overexpression and knockdown cell lines. Meanwhile, the expression plasmids of *Furin* and *ANGPTL4* were constructed using a pCDNA3.1 vector (MiaoLing Biology, Wuhan, Hubei, China). Site-directed mutagenesis was performed by an overlap extension polymerase chain reaction to generate *ANGPTL4* S30A mutants, where the serine 30 residue (Ser30) was substituted for Ala (MiaoLing Biology, Wuhan, Hubei, China). To construct 6×His-tagged, 3×Flag-tagged, and 3×Myc expression plasmids, the inserts of the above His-tagged *ANGPTL4* (His-ANGPTL4), Flag-tagged *LPL* (Flag-LPL), or Myc-tagged inositol-requiring enzyme-1 (Myc-IRE1) expression plasmids were subcloned into the pCMV vector (MiaoLing Biology). The transfection techniques were carried out as previously reported and in accordance with the manufacturer's instructions [30]. Briefly, for each well of a 6-well plate, 100 pmol siRNA or 2.5 μg plasmids were transfected into cells using Lipofectamine 3000 (Invitrogen, CA, USA). The specific sequences of the siRNA or shRNA mentioned above can be found in Supplementary Table S1.

2.3 | Antibody and Western blotting (WB)

GC cells or tissues were lysed using the radioimmunoprecipitation assay (RIPA) lysis buffer (Beyotime, Shanghai, China), followed by sonication of the cell lysate at a frequency of 20 kHz. The protein sample (30 μg) was then electrophoresed in a tris-glycine electrophoresis system (Tanon, Shanghai, China), followed by the transfer of the target bands onto 0.45 μm polyvinylidene fluoride membranes (Cytiva, Amersham, Buckinghamshire, United Kingdom) and visualization using a

chemiluminescent detection system (Tanon, Shanghai, China). The detailed information on antibodies is summarized in Supplementary Table S2.

2.4 | Oil red O staining and immunohistochemistry (IHC)

According to a previously established protocol for IHC [17], collected tissues were fixed using 4% paraformaldehyde. Paraffin sections were prepared, followed by antigen retrieval with citrate-EDTA solution (Beyotime, Shanghai, China) after dewaxing treatment. The sections were treated with blocking buffer (Beyotime) to reduce the background and then incubated overnight at 4°C with primary antibodies. Horseradish peroxidase-labeled secondary antibodies (Maxim Biotechnologies, Fuzhou, Fujian, China) were used. Finally, the sections were exposed to diaminobenzidine for 5 min, lightly counterstained with hematoxylin. The primary antibodies employed for IHC were summarized in Supplementary Table S2. We calculated a staining index of IHC based on the staining intensity and the number of positively stained GC cells using a method described by others [31].

Oil red O staining was performed per the manufacturer's protocol (Beyotime, Shanghai, China). In brief, tissue sections were incubated with washing buffer for 20 s and then covered with the working solution at room temperature for 30 min. Nuclei were counterstained with hematoxylin for 3 min. The ImageJ software (National Institutes of Health, Bethesda, MD, USA) was used to calculate the oil red O staining area of the samples. The cutoff values distinguishing high or low staining of the interested proteins and oil red O staining were determined based on the median of all samples.

2.5 | Flow cytometric analysis

Flow cytometry was employed for quantitative analysis of BODIPY 493/503 and Dil-VLDL staining in GC cells, which aimed to investigate the impact on intracellular lipid levels or the uptake of VLDL, respectively. Firstly, 5×10^5 treated cells were seeded onto a 6-well plate and stained upon reaching 80%-90% confluency. The cells were incubated at 37°C for 15 min with 2 μmol/L BODIPY 493/503 staining solution (GlpBio Technology, Montclair, CA, USA) or incubated at 37°C for 2 h with 5 μg/mL Dil-VLDL staining solution (Kalen Biomedical, Montgomery Village, MD, USA). Subsequently, equal amounts of cells were harvested, and their fluorescence intensity was measured using a flow cytometer (CytoFlex, Beckman Counter, Shanghai, China).

2.6 | Immunofluorescence

Immunofluorescence was conducted according to a previous study [32]. Briefly, cells were fixed with 4% paraformaldehyde for 15 min and washed three times with phosphate-buffered saline. Non-specific binding was blocked with normal goat serum (Beyotime, Shanghai, China). Then, cells were incubated with the primary antibody overnight at 4°C (Supplementary Table S2). FITC- or Cy3-labeled goat anti-rabbit/mouse IgG secondary antibody was used to visualize the immunoreactivity (Beyotime, Shanghai, China). Afterward, the cells were treated with 2-(4-Amidinophenyl)-6-indolecarbamidine dihydrochloride (DAPI) (Beyotime, Shanghai, China) for nuclear staining and imaged under an immunofluorescence microscope (THUNDER DMi8, Leica, Wetzlar, Germany).

2.7 | Lipidomic analysis

MKN45 cells transfected with *LPL* siRNA or control oligonucleotides were harvested and rapidly frozen with liquid nitrogen before lipidomic analysis. The lipidomic analysis was conducted by Suzhou PANOMIX Biomedical Tech Co., Ltd. (Suzhou, Jiangsu, China). The liquid chromatographic analysis was performed on a Vanquish UHPLC system (Thermo Fisher Scientific, Waltham, MA, USA). Mass spectrometric detection of metabolites was performed on Q Exactive (Thermo Fisher Scientific, Waltham, MA, USA). In short, 750 μL of mixed solvent (chloroform: methanol, 2:1, v/v) and 100 mg of glass beads were added to each cell pellet, and that sample mixture was vortexed. The samples were then frozen in liquid nitrogen for 5 min and thawed on ice. After centrifuging at room temperature for 5 min, the organic layer was removed and transferred to a new tube. The collected organic layer was concentrated by a vacuum concentrator, dissolved by isopropyl alcohol, and filtered by a 0.22 μm membrane to obtain the prepared sample for liquid chromatography-mass spectrometry.

2.8 | HLEC tube formation assay

HLECs (1×10^4 cells per well) suspended in conditional medium (CM) or control complete medium were added to a 96-well plate pre-coated with 50 μL matrigel (Corning, Bedford, MA, USA). After 4 h of incubation at 37°C, the formation of a network was observed under a microscope (Zeiss, Oberkochen, Germany). The total branching tube lengths per unit area were quantified using the Angiogenesis Analyzer plugin of the ImageJ software.

2.9 | Co-immunoprecipitation (Co-IP) assay

The Co-IP assay was performed using an immunoprecipitation kit with protein A+G magnetic beads (Beyotime). In brief, the primary antibody or tag antibody was incubated with protein A+G magnetic beads on a rotary mixer at room temperature for 30 min (Supplementary Table S2). Next, the sample lysate was mixed with beads conjugated with antibodies and incubated overnight at 4°C. After that, the precipitated beads were eluted with sodium dodecyl sulfate loading buffer after washing. The eluted protein complexes were then detected by WB or silver staining (Beyotime, Shanghai, China). Additionally, precipitated proteins were also sent to high-performance liquid chromatography-tandem mass spectrometry (HPLC-MS/MS) analysis on a RIGOL L-3000 system (Beijing RIGOL Technology, Beijing, China). Of note, because the detection of 50 kDa or 25 kDa proteins on WB after immunoprecipitation often suffers from heavy or light chain blotting contamination, we used specific secondary antibodies to eliminate heavy or light chain interference (Abbkine, Atlanta, GE, USA).

2.10 | Glutathione-S-transferase (GST)-tagged protein purification and GST pull-down assays

GST-IRE1, encoded by the plasmid pGEX-4T-1 (MiaoLing Biology, Wuhan, Hubei, China), was expressed in Escherichia coli BL21 (MiaoLing Biology) through induction with 0.5 mmol/L isopropyl β-d-1-thiogalactopyranoside (Beyotime, Shanghai, China) and was then purified using magnetic glutathione-sepharose beads (BersinBio, Guangzhou, Guangdong, China).

For the GST pull-down assay, GST or GST-IRE1 bound to glutathione-sepharose beads were incubated overnight with protein lysates from His-ANGPTL4-expressed GC cells at 4°C. After being washed with phosphate-buffered saline with 0.05% Tween 20 (PBST) three times, the complexes were eluted with sodium dodecyl sulfate loading buffer. The collected elution fractions were then subjected to WB analysis using the indicated antibodies (Supplementary Table S2).

2.11 | Mouse popliteal LNM model

In this study, 4-week-old female BALB/c nude mice were purchased from the Experimental Animal Center of Nanjing Medical University (Nanjing, Jiangsu, China) and housed in specific pathogen-free barrier facilities. All mice were fed on either a control diet (CD; total energy: 4,057 kcal/kg; 10% energy from fat, 20% protein, and 70% carbohydrate; D12450J, OpenSource Diets, New Brunswick, NJ, USA) or an HFD (total energy: 5,242.95 kcal/kg; 60% energy from fat, 20% protein, and 20% carbohydrate; D12492, OpenSource Diets). We inoculated lentivirus-transduced MKN45 cells (2×10^6 cells) that stably expressed firefly luciferase into the footpads of the mice. Lymph drainage in the footpad is directional with the popliteal and subsequent to the external iliac nodes and the common iliac lymph nodes (LNs), which enables more sensitive and quantitative In vitro measurements of LNMs. Popliteal LNM was monitored and imaged weekly using a bioluminescence imaging system (PerkinElmer, IVIS Spectrum Imaging System, Waltham, MA, USA). At 8 weeks after injection, mice were euthanized, the primary tumors and popliteal LNs were excised and subjected to hematoxylin-eosin (H&E) staining, IHC, or oil red O staining. For H&E staining, paraffin-embedded tissues were sectioned, deparaffinized by xylene, anhydrous ethanol, 90% alcohol, 80% alcohol, 70% alcohol, and distilled water. Then, slides were stained with hematoxylin for 5 min and eosin for 1 min (Beyotime, Shanghai, China). The LN volumes were calculated using the following formula: LN volume (mm^3) = (length [mm]) × (width [mm])^2 × 0.52. Celecoxib was dissolved in the drinking water (calculated as 8 mg/kg daily). Administration of celecoxib was started in the second week after cell injection and discontinued 4 weeks later.

2.12 | In vitro phosphorylation assay and Phos-tag sodium dodecyl-sulfate polyacrylamide gel electrophoresis (SDS-PAGE)

GC cells were transfected with either His-tagged wild-type or S30A-mutated ANGPTL4 plasmids (MiaoLing Biology, Wuhan, Hubei, China) for 48 h. Then, ANGPTL4 protein was precipitated with anti-His antibody-coated magnetic beads (Vazyme, Nanjing, Jiangsu, China) at 4°C overnight on a rocker. Afterward, purified ANGPTL4 proteins were then incubated with recombinant active human IRE1 (E31-11G, SignalChem, Richmond, British Columbia, Canada) in kinase assay buffer (K01-09, SignalChem) supplemented with 200 μmol/L adenosine triphosphate at 30°C for 45 min. The reaction mixture was then boiled in an SDS loading buffer (Beyotime, Shanghai, China) at 95°C and loaded to Phos-tag SDS-PAGE (Wako, Osaka, Japan) according to the manufacturer's instructions. In the Phos-tag-containing gel, the phosphorylated protein migrated

more slowly than the corresponding dephosphorylated forms.

2.13 | Reagent

Recombinant human leptin, recombinant human interleukin-6 (IL-6), and recombinant human insulin-like growth factor 1 (IGF-1) were obtained from Beyotime Biotechnology (Shanghai, China). Arachidonic acid (AA) and PGE2 were acquired from Aladdin Biochemical Technology (Shanghai, China). Fatty acid-free bovine serum albumin (BSA) was purchased from Maokang Biotechnology (Shanghai, China). VLDL was purchased from Yiyuan Biotechnology (Guangzhou, Guangdong, China). Celecoxib, AMG-18, bafilomycin A1, brefeldin A, and thapsigargin were obtained from Selleck (Shanghai, China). Fat emulsion (FE) was used to treat cells (C6-24, Fresenius KABI, Beijing, China)

2.14 | Cell migration assay

The migrative capacity of GC cells and HLECs was assessed using the transwell system (Corning, Bedford, MA, USA). In brief, 2×10^4 cells were seeded in the upper chamber with serum-free culture medium, while the lower chamber was filled with 500 μL of complete medium or conditional medium derived from GC cells.

2.15 | Cell proliferation assay

We measured cell growth by EdU incorporation assay and colony formation assay. The detailed experimental procedures have been delineated in our previous studies [32, 33]. Briefly, 500 cells per well were seeded in a 6-well plate, and the cell colonies were stained with crystal violet (Beyotime, Shanghai, China) 2 weeks later. For the EdU incorporation assay, 5×10^3 cells per well were seeded in a 96-well plate. Then, cells were incubated with the EdU dye (Ribo-Bio, Guangzhou, Guangdong, China) and visualized under a fluorescence microscope (Nikon, Tokyo, Japan).

2.16 | Enzyme linked immunosorbent assay (ELISA)

The circulating level of leptin in the plasma of 57 GC patients was detected using the Human Leptin ELISA Kit (Elabscience, Wuhan, Hubei, China). The expression of PGE2 and AA in cell lysate, cell supernatant, and tissue homogenates was respectively evaluated using the PGE2 ELISA Kit (Elabscience) or the AA ELISA Kit (Elabscience).

2.17 | Bioinformatic analyses

RNA-seq data for 34 GC cell lines were downloaded from the Cancer Cell Line Encyclopedia (CCLE) database (https://sites.broadinstitute.org/ccle). Based on the expression of LPL in GC cell lines, we performed Gene Set Enrichment Analysis (GSEA) to reveal LPL-related pathways or functions (GSEA v4.1.0, Broad Institute, San Diego, CA, USA). Using the data from The Cancer Genome Atlas Program (TCGA), the overall survival (OS) and recurrence-free survival (RFS) curves of LPL were downloaded from the Kaplan-Meier Plotter [34].

2.18 | Statistical analysis

Statistical analysis was conducted using GraphPad Prism 6 (GraphPad Software, San Diego, CA, USA). A student's *t*-test (two-tailed) was used to compare two groups. Pearson analysis was employed to examine correlations between measured variables. The mean ± standard deviation (SD), derived from three independent experiments, is represented by error bars. $P < 0.05$ indicated significant differences.

3 | RESULTS

3.1 | N+ GC exhibited elevated levels of intracellular lipids and LPL expression

Using oil red O staining, we found that N+ GC tissues exhibited higher levels of lipid accumulation than N0 GC tissues, and cancerous tissues also showed higher lipid storage than adjacent normal tissues (Figure 1A-B). Subsequently, IHC analysis of 57 paired tissues revealed significantly higher expression of LPL in N+ GC tissues than N0 GC tissues (Figure 1C-D). Additionally, N+ GC tissues showed an increased density of lymphatic vessels, as revealed by LYVE-1 staining, in comparison to N0 GC tissues (Figure 1E-F). Correlation analysis further established positive associations between LPL expression, lipid accumulation, and lymphatic vessel density (Figure 1G-I). WB experiments also showed that GC cells and tissues had substantially higher expressions of LPL than did normal cells, GES-1, and matching tissues (Figure 1J-K). Notably, it also unveiled the occurrence of LPL cleavage in GC, characterized by the detection of N-terminal fragments of LPL measuring approximately 35 kDa (Figure 1J-K). Previous

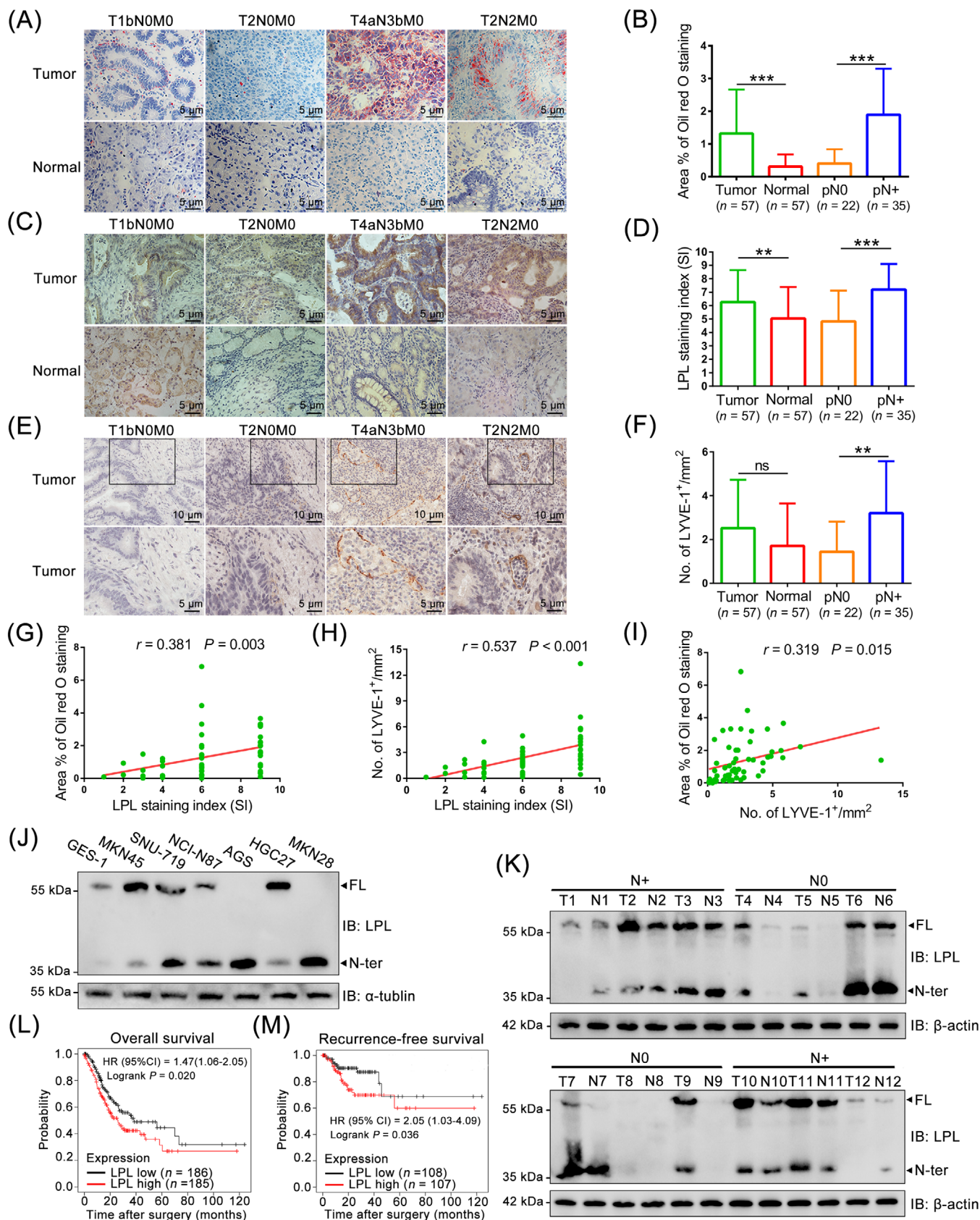FIGURE 1   N+ GC exhibited elevated levels of intracellular lipids and LPL expression. (A-B) Representative images (A) and quantification (B) of oil red O staining areas in the frozen tumor sections and adjacent normal sections of GC, with or without LNM. Scale bar, 5 μm. (C-D) Representative IHC images (C) and quantification (D) of LPL expression in 57 paired tumor tissues and normal tissues. Scale

studies have indicated that the intracellular cleavage of LPL in adipocytes generated N-terminal fragments measuring 35.3 kDa and C-terminal fragments measuring 18 kDa, ultimately leading to impaired LPL activity followed by lysosomal degradation of LPL [35, 36]. Therefore, the absence of LPL expression in AGS and MKN28 cells could be attributed to its cleavage (Figure 1J). Moreover, survival analyses revealed significant associations between high expression levels of LPL and unfavorable OS (hazard ratio [HR] = 1.47, P = 0.020) and RFS (HR = 2.05, P = 0.036) (Figure 1L-M).

3.2 | Exogenous lipids or an HFD could promote the expression of LPL and LNM in GC

GC cells were treated with VLDL or FE, which can provide exogenous lipids. Meanwhile, cells were cultured in a low-glucose medium to minimize de novo lipid synthesis (Supplementary Figure S1A). Compared with cells cultured in low-glucose medium with 1% BSA, those treated with 0.1% FE or VLDL showed enhanced levels of lipid deposition (Supplementary Figure S1B). We then used flow cytometry to measure the basal lipid level in GC cells. The results revealed that AGS and MKN28 had the lowest lipid levels, whereas MKN45 and HGC27 contained higher levels, showing the same pattern as LPL expression in GC cells (Supplementary Figure S1C). Moreover, exogenous lipid treatment could increase the expression of LPL (Supplementary Figure S1D-E), highlighting the role of LPL in lipid uptake. Next, we investigated the biological function of exogenous lipids in GC. EdU incorporation and transwell assays indicated that the accumulation of lipids contributed to the proliferation and dissemination of GC cells (Supplementary Figure S2A-B). Remarkably, it also increased the promotional effect of GC cells in inducing HLEC tube formation (Supplementary Figure S2A-B), indicating the requirement of lipids in GC lymphangiogenesis.

The HFD mouse model is a well-established method for investigating the effect of dietary lipids or obesity on tumor metastasis. Besides, an in vivo nude mouse popliteal LNM model was employed (Supplementary Figure S2C). It was found that the HFD clearly promoted MKN45 cell LNM, as determined by luminescence intensity (Supplementary Figure S2D). The primary footpad tumors and popliteal LNs were dissected and collected, and all dissected popliteal LNs were validated by H&E staining (Supplementary Figure S2E). The volumes of LNs were notably larger in the HFD tumor group than in the CD group (Supplementary Figure S2F). In addition, compared with the CD group, primary footpad tumors from the HFD group also showed enhanced oil red O staining area and elevated expression of LPL (Supplementary Figure S2G). Consistently, WB analyses also detected a higher expression level of LPL in the HFD group (Supplementary Figure S2H). Collectively, these results demonstrated that an HFD promoted the expression of LPL and LNM in GC.

3.3 | Upregulated expression of LPL promoted the uptake of exogenous lipids

LPL is essential for lipid transportation and utilization. Nevertheless, the role of LPL in cancer remains unclear. To this end, MKN45 and HGC27 cells were transfected with LPL-targeting siRNA, LPL-targeting shRNA, LPL overexpression vector, or lentiviruses carrying control shRNA/empty vector (Figure 2A-C). The BODIPY fluorescence intensity of MKN45 and HGC27 cells was measured by flow cytometry. It showed that LPL knockdown markedly decreased intracellular lipid levels, while LPL restoration notably promoted the storage of lipids in VLDL-treated GC cells (Figure 2D-E). To further confirm the role of LPL in stimulating exogenous lipid uptake, we used Dil-labeled VLDL as the tracker of exogenous lipid uptake. Both flow cytometry and fluorescence images demonstrated that the reduction of LPL expression restricted the uptake of Dil-VLDL (Figure 2F-I).

bar, 5 μm. (E-F) LYVE-1⁺ lymphatic vessel densities were visualized (E) and quantified (F) in tumor sections of GC. Scale bar, 10 μm (upper panel) and 5 μm (lower panel). (G-I) Pearson analyses were conducted between LPL expression and oil red O staining area (G), LPL expression and LYVE-1⁺ vessel densities (H), and oil red O staining area and LYVE-1⁺ vessel densities (I). (J-K) WB analysis of GC cell lysates (J) and GC tissue homogenates (K) using an antibody against the N-terminal fragment of human LPL. (L-M) Kaplan-Meier survival analysis of the OS (L) and RFS (M) of GC patients with low versus high LPL expression in the TCGA cohort. The cutoff value is the median of LPL expression. The data were presented as the mean ± SD. The P value was calculated by the t test (B, D, and F), Pearson correlation analysis (G, H, and I), or log-rank test (L and M). **P < 0.01, ***P < 0.001, ns, not significant. Abbreviations: FL, full-length; GC, gastric cancer; HR, hazard ratio; IB: immunoblotting; IHC, immunohistochemistry; LNM, lymph node metastasis; LPL, lipoprotein lipase; LYVE-1, lymphatic vessel endothelial hyaluronan receptor 1; N, normal; N+, node-positive; N0, node-negative; N-ter, N-terminus; OS, overall survival; RFS, recurrence-free survival; SD, standard deviation; T, tumor; TCGA, The Cancer Genome Atlas.
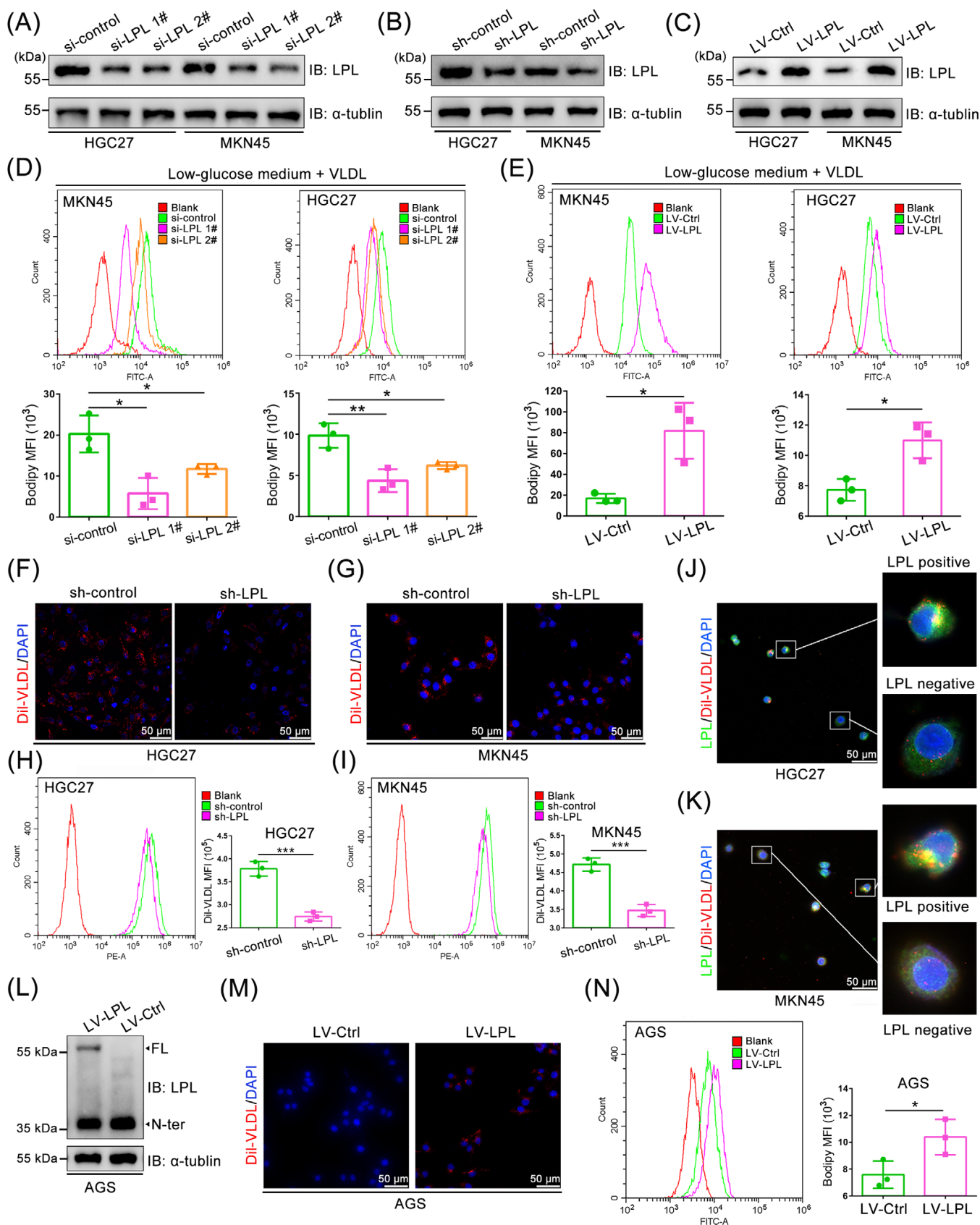
FIGURE 2 LPL promoted the uptake of exogenous lipids. (A-B) Cellular LPL was effectively downregulated using LPL-targeting siRNAs (A) or shRNAs (B) in HGC27 and MKN45 cells. (C) The expression of LPL was overexpressed in HGC27 and MKN45 cells. (D-E) MKN45 and HGC27 cells with LPL knockdown (D) or overexpression (E) were cultured in a low-glucose medium with VLDL (25 μg/mL) for 24 h. Then,

Meanwhile, fluorescence images revealed increased fluorescence intensities of Dil-VLDL in LPL-positive cells than in LPL-negative GC cells (Figure 2J-K). Furthermore, we used the AGS cell line characterized by the absence of full-length LPL expression to consolidate the above phenomena (Figure 2L). The fluorescence presentation of Dil-VLDL uptake in LPL-overexpressing AGC cells confirmed the dependence of VLDL uptake on active LPL (Figure 2M). Overexpression of full-length LPL in AGS cells also improved intracellular lipid levels (Figure 2N). Taken together, all the data suggest that LPL mediates lipid uptake in GC cells.

3.4 | LPL promoted LNM of GC

Tumor-associated lymphangiogenesis is a rate-limiting step for the LNM of cancer [37]. Hence, we explored the effect of LPL on lymphangiogenesis by co-culturing HLECs with CM from GC cells. Co-culture with CM from LPL-silenced HGC27 or MKN45 cells attenuated HLEC tube formation and migration as compared with the control cells (Figure 3A-B, Supplementary Figure S3A, and Supplementary Figure S4A). Conversely, HLECs showed an upregulation of tube formation and migration after co-culture with the CM derived from LPL-overexpressing GC cells (Figure 3C-D, Supplementary Figure S3B, and Supplementary Figure S4B). In addition, the effect of LPL on HLEC tube formation and cell migration was augmented when GC cells were treated with VLDL (Figure 3A-D, Supplementary Figures S3-S4). The enhanced invasiveness and proliferation of tumor cells are also vital for stimulating tumor LNM. We found that VLDL treatment significantly promoted GC cell proliferation and migration, and this effect was mediated by LPL (Supplementary Figures S3-S4).

We then used the popliteal LNM model to validate the function of LPL in vivo. Considering the promoting effect of HFD on LNM and the crucial role of LPL in lipid uptake, we initially conducted an experiment where LPL-silenced cells were injected into the footpads of mice fed on an HFD. The results showed that LPL knockdown significantly inhibited the metastasis of MKN45 cells to the LNs (Figure 3E). In contrast, overexpression of LPL promoted LNM in mice fed on a CD, as determined by in vivo imaging systems (Figure 3F). Accordingly, the volumes of popliteal LNs were strikingly smaller in the LPL knockdown mice but larger in the LPL overexpressing mice than in the corresponding control mice (Figure 3G-H). Metastatic LNs were confirmed by H&E staining, and the level of oil red O staining and LPL expression was measured in primary footpad tumors. We found that overexpression of LPL in the CD group promoted the rate of popliteal LN metastasis, increased the area of oil red O staining, and enhanced LPL expression, while LPL knockdown in the HFD group reversed these effects (Figure 3I-L). Taken together, these findings suggest that LPL promotes LNM of GC by mediating lipid uptake.

3.5 | Leptin impaired ANGPTL4/Furin-mediated cleavage of LPL

Given the ability of LPL to make free fatty acids available to adipose tissues, LPL is considered to play a central role in the pathogenesis of obesity [38]. Several molecular mechanisms, such as cancer-associated adipocytes, obesity-related inflammatory cytokines (e.g., IL-6), lipids, adipokines (e.g., leptin and adiponectin), IGF-1, and sex hormones, have been proposed to explain the association between obesity and cancer [39]. Hence, we investigated the possible role of obesity-related factors (IL-6, leptin, and IGF-1) in regulating LPL expression. The WB results demonstrated that leptin treatment with increasing concentrations promoted the expression of full-length LPL while accompanied by a decrease in the expression of LPL N-terminus, but this effect was not observed with IGF-1 or IL-6 treatment (Figure 4A and Supplementary Figure S5A). Meanwhile, MKN45 and HGC27 were exposed to different time periods of leptin, and the results showed that a

intracellular lipid was stained by BODIPY 493/503 (2 μmol/L) and determined by flow cytometry. (F-G) The uptake of Dil-VLDL (5 μg/mL) in HGC27 (F) and MKN45 (G) cells treated with LPL shRNA was detected by fluorescence. Scale bar, 50 μm. (H-I) Flow cytometry was used to analyze Dil-VLDL (5 μg/mL) uptake in HGC27 (H) and MKN45 (I) cells with LPL knockdown. (J-K) Representative images of LPL localization and Dil-VLDL intensity in HGC27 (J) and MKN45 (K) cells treated with LPL shRNA. Scale bar, 50 μm. (L) The expression of full-length LPL was overexpressed in AGS cells. (M) AGS cells with expression of full-length LPL or native AGS cells were incubated with Dil-VLDL (5 μg/mL) for 2 h, and then the fluorescence intensity of Dil-VLDL in the cells was detected. Scale bar, 50 μm. (N) Flow cytometric analysis showed enhanced lipid levels in LPL-overexpressing AGS cells. The data were presented as the mean ± SD. The P value was calculated by paired t test (D, E, H, I, and N). *$P < 0.05$, **$P < 0.01$, ***$P < 0.001$. Abbreviations: FL, full-length; GC, gastric cancer; IB, immunoblotting; LPL, lipoprotein lipase; LV-Ctrl, negative control lentivirus vector; LV-LPL, LPL overexpression lentivirus vector; N-ter, N-terminus; SD, standard deviation; sh-LPL, short hairpin RNA of LPL; sh-NC, negative control short hairpin RNA; si-control, negative control small interfering RNA; si-LPL, small interfering RNA of LPL; VLDL, very low-density lipoproteins.
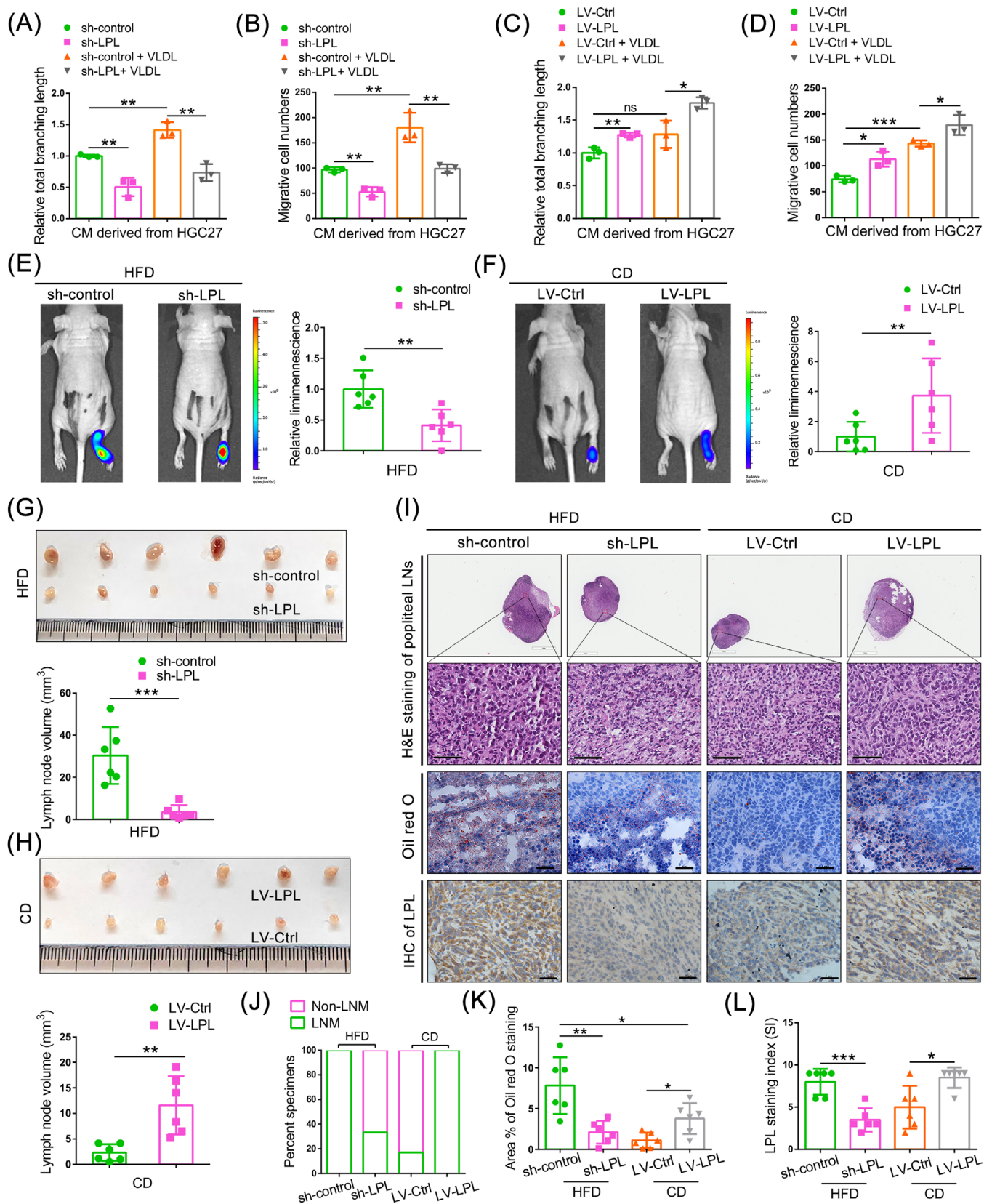
FIGURE 3 LPL promoted lymphatic metastasis of GC. (A-B) Quantification of the tube formation (A) and transwell migration (B) of HLECs cocultured with CM derived from HGC27 cells treated with LPL shRNA and/or VLDL. (C-D) Tube formation (C) and cell migration (D) were analyzed in HLECs cocultured with CM derived from HGC27 cells treated with LPL expression vectors and/or VLDL. (E-F) Representative images of bioluminescence and histogram analysis of popliteal LN metastasis in the HFD-fed (E) and CD-fed (F) mouse

4-hour treatment could yield a favorable induction effect (Figure 4B and Supplementary Figure S5B). Significantly, the WB result also revealed a correlation between elevated circulating leptin levels and reduced LPL cleavage levels in GC tissues (Figure 4C). As LPL is a secreted protein and its secretion can impact the expression pattern of LPL in cells, we employed brefeldin A as a secretion blocker to inhibit the release of LPL while exposing GC cells to leptin [40]. Our findings demonstrated that leptin suppressed the cleavage of LPL regardless of whether protein secretion was inhibited or not (Figure 4D and Supplementary Figure S5C). Thus, these results indicate that leptin treatment is able to inhibit the intracellular cleavage of LPL.

The cleavage of LPL by Furin is triggered by the ANGPTL4-induced unfolding of LPL [36]. Hence, to confirm that the cleavage of LPL in GC cells is also processed by the ANGPTL4/Furin axis, we introduced ANGPTL4-targeting siRNAs or Furin-overexpressing vectors into GC cells. The results demonstrated that ANGPTL4 knockdown attenuated LPL cleavage while overexpression of Furin significantly promoted it (Figure 4E-G). Co-IP analysis revealed the binding of ANGPTL4 and Furin to flag-tagged LPL in HGC27 cells (Figure 4H). Previous studies have shown that N-terminal LPL is cleared by lysosomes [36]. Therefore, after transfection of the Furin/ANGPTL4 overexpressing vector or control vector for 48 h, we added the lysosomal degradation inhibitor bafilomycin A1 to exclude the effect of lysosomal degradation on the expression of N-terminal LPL in GC cells. Our results indicated that overexpression of either Furin or ANGPTL4 reversed leptin-induced inhibition of LPL cleavage (Figure 4I-J and Supplementary Figure S5D-E). However, leptin did not affect the expression of ANGPTL4 and Furin in GC cells (Figure 4K and Supplementary Figure S5F). Of note, immunofluorescent analysis showed that there was significant co-localization between ANGPTL4 and LPL in GC cells, whereas leptin treatment profoundly reduced their co-localization (Figure 4L and Supplementary Figure S5G). Leptin exerts its effect through LEPR expressed in the brain and peripheral tissues [41]. Therefore, we further evaluated whether the effect of leptin on LPL cleavage is dependent on LEPR. LEPR knockdown markedly diminished the effect of leptin on LPL cleavage

(Figure 4M and Supplementary Figure S5H). Therefore, these results indicate that the leptin-LEPR pathway could inhibit ANGPTL4/Furin-mediated cleavage of LPL.

3.6 | Leptin induced ANGPTL4 phosphorylation in an IRE1 kinase-dependent manner

In comparison to untreated cells, leptin treatment resulted in a significant reduction in the binding affinity of LPL with ANGPTL4 and Furin (Figure 5A), suggesting a dissociation between ANGPTL4 and LPL caused by leptin treatment. Silver staining assay and mass spectrometric analysis of immunoprecipitants of His-ANGPTL4 showed that leptin may induce an association between IRE1 and ANGPTL4 (Figure 5B, Supplementary Figure S6A, and Supplementary Table S3). WB analysis further confirmed that exogenously expressed His-ANGPTL4 could bind to IRE1 (Figure 5C and Supplementary Figure S6B). Moreover, the interaction of endogenous ANGPTL4 with IRE1 was also observed (Figure 5D and Supplementary Figure S6C). Compared to the control group, leptin treatment also induced the co-localization between ANGPTL4 and IRE1 (Figure 5E and Supplementary Figure S6D). The interaction between ANGPTL4 and IRE1 was further validated through In vitro GST pull-down assays, wherein purified GST-IRE1 was co-incubated with purified His-ANGPTL4. The specific binding of His-ANGPTL4 to immobilized GST-IRE1, as opposed to GST alone, confirmed the direct interaction between IRE1 and ANGPTL4 (Figure 5F). Additionally, immunoprecipitation with an anti-IRE1 antibody demonstrated the interaction between endogenous IRE1 and ANGPTL4 in leptin-treated GC cells (Figure 5G and Supplementary Figure S6E). Subsequent sequential immunoprecipitation experiments further confirmed the association between Myc-IRE1 and His-ANGPTL4 in leptin-treated GC cells (Supplementary Figure S6F-G). Hence, these findings unequivocally illustrate the capacity of leptin to stimulate IRE1 binding to ANGPTL4.

IRE1, also known as endoplasmic reticulum to nucleus signaling 1 (ERN1), comprises two functional catalytic domains: a serine/threonine-protein kinase domain and

---

groups ($n = 6$ per group). (G-H) Representative images of the enucleated popliteal LN and histogram analysis of the LN volume ($n = 6$ per group) in the HFD group (G) and CD group (H). (I-L) Representative images (I) and histogram analyses of popliteal LN status (J), oil red O staining area (K), and LPL staining index (L). Scale bars for H&E staining were 1 mm (2×) or 60 μm (40×); scale bar for oil red O and IHC staining were 5 μm. The data were presented as the mean ± SD. The P value was calculated by paired t test. *$P < 0.05$; **$P < 0.01$; ***$P < 0.001$, ns, not significant. Abbreviations: CD, control diet; CM, conditional medium; GC, gastric cancer; HFD, high-fat diet; HLEC, human lymphatic endothelial cell; IHC, immunohistochemistry; LNM, lymph node metastasis; LPL, lipoprotein lipase; LV-Ctrl, negative control lentivirus vector; LV-LPL, LPL overexpression lentivirus vector; SD, standard deviation; sh-LPL, short hairpin RNA of LPL; sh-NC, negative control short hairpin RNA; VLDL, very low-density lipoproteins.
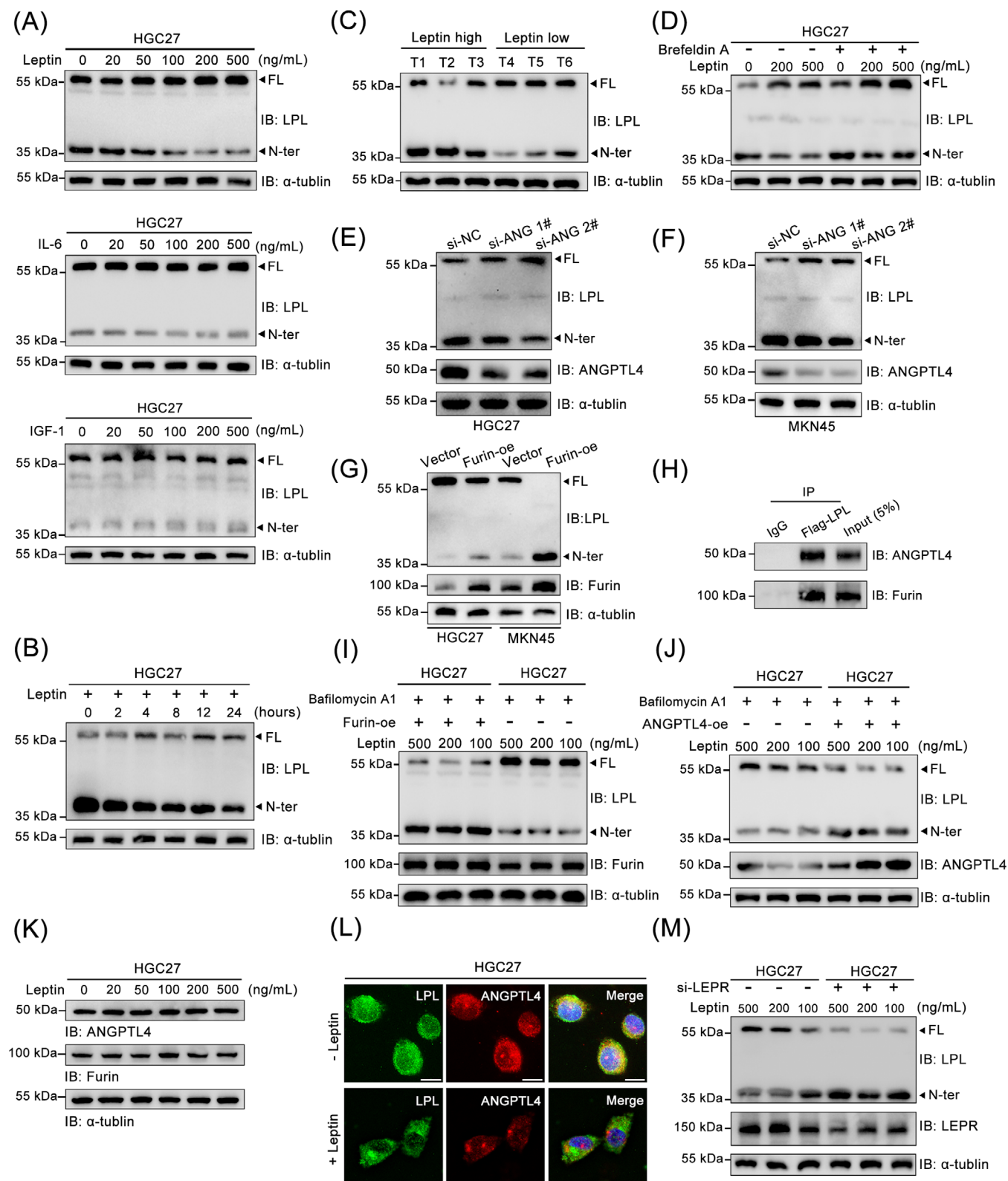
FIGURE 4 Leptin impaired ANGPTL4/Furin-mediated cleavage of LPL. (A) WB analysis was performed on HGC27 cell lysates that were treated with increasing concentrations of leptin, IL-6, or IGF-1 for a duration of 4 h. (B) WB analysis was conducted on HGC27 cells subjected to leptin treatment (200 ng/mL) at specified time intervals. (C) Detection of LPL cleavage in GC tissues with high or low serum leptin levels by WB. (D) HGC27 cells were treated with Brefeldin A (1 μg/mL, 1 h) and increasing concentrations of leptin (4 h), and then the cleavage of LPL was detected by WB. (E-F) Detection of LPL cleavage in HGC27 (E) and MKN45 (F) cells that were transfected with ANGPTL4-targeting siRNAs or control siRNAs for 48 h by WB. (G) Detection of LPL cleavage in Furin-overexpressing GC cells by WB. (H)

an endoribonuclease domain, being one of the crucial drivers of the unfolded protein response [42]. Based on the mass spectrometric data from PhosphoSitePlus [43], IRE1 emerged as the kinase with a high score for potential phosphorylation of ANGPTL4 at the Ser30 residue (Figure 5H). Using an antibody against phosphoserine, we assessed the expression of phosphoserine in the immunoprecipitants from endogenous ANGPTL4, exogenous His-ANGPTL4, or normal IgG. As anticipated, we exclusively detected the presence of phosphoserine (50 kDa) in the group treated with leptin (Figure 5I-J and Supplementary Figure S6H-I). Besides, in the immunoprecipitants from endogenous IRE1, we also detected the expression of phosphoserine in the leptin-treated group (Figure 5K and Supplementary Figure S6J). However, additional bands at approximately 100 kDa alongside the band at 50 kDa were detected. We believe that the band at 50 kDa likely represented phosphorylated serine of ANGPTL4, while the bands around 100 kDa potentially indicated phosphorylated serine of IRE1. So far, we can assume that leptin can cause serine phosphorylation of ANGPTL4 and that this process is mediated by IRE1. Mutation of Ser30 in ANGPTL4 to alanine (S30A) or treatment with an IRE1 kinase-specific inhibitor (AMG-18) abolished leptin-induced phosphorylation of ANGPTL4 (Figure 5L-M and Supplementary Figure S6K). Moreover, stimulation of IRE1 kinase activity by thapsigargin also promptly induced the phosphorylation of ANGPTL4 in HGC27 cells (Supplementary Figure S6L). To confirm the direct phosphorylation of ANGPTL4 by IRE1, we employed In vitro phosphorylation assays accompanied by Phostag electrophoresis. The results showed the S30A-mutated ANGPTL4, expressed in MKN45 and HGC27 cells, were resistant to phosphorylation that was induced by IRE1 kinase, and this phosphorylation of Ser30 in this reaction was in an AMG-18-sensitive manner (Figure 5N and Supplementary Figure S6M). IRE1 has been described as a protein that undergoes trans-autophosphorylation to activate its RNase and kinase activities [44]. Utilizing a specific antibody targeting Ser724 phosphorylation on IRE1, we observed that leptin significantly induced IRE1 autophosphorylation without affecting the level of IRE1 protein

(Figure 5O and Supplementary Figure S6N). Thus, these results indicated that leptin induced the autophosphorylation of IRE1, which then phosphorylated ANGPTL4 at the Ser30 residue.

3.7 | The signaling of leptin-LEPR-IRE1-ANGPTL4 suppressed LPL cleavage while promoting lipid accumulation

We next investigated the impact of ANGPTL4 phosphorylation on LPL cleavage. First, leptin treatment effectively inhibited LPL cleavage, and this inhibitory effect was nullified in GC cells transduced with S30A mutants (Figure 6A; Supplementary Figure S7A). Additionally, AMG-18 also markedly decreased the impact of leptin on LPL cleavage (Figure 6B; Supplementary Figure S7B). Furthermore, the expression of S30A mutants also counteracted the inhibitory effect of thapsigargin on LPL cleavage (Figure 6C; Supplementary Figure S7C). Notably, wild-type ANGPTL4, but not S30A-mutated ANGPTL4, that was immunoprecipitated from leptin-treated HGC27 cells showed a reduction in binding to LPL (Figure 6D). Similarly, the S30A mutants also blocked the leptin-induced loss of co-localization between ANGPTL4 and LPL (Figure 6E; Supplementary Figure S7D). These findings strongly suggest that IRE1-mediated phosphorylation of ANGPTL4 diminishes its affinity for LPL, thereby inhibiting LPL cleavage.

Compared to N0 cases, the serum of N+ patients exhibited a significant upregulation in circulating leptin levels, as determined by ELISA assays (Figure 6F). Moreover, correlation analyses demonstrated positive correlations between circulating leptin levels and LPL expression ($r = 0.442$, $P < 0.001$), oil red O staining area ($r = 0.341$, $P = 0.009$), as well as the BMI index ($r = 0.302$, $P = 0.029$) (Figure 6G-I). The IHC results also demonstrated a significantly elevated expression level of LEPR in N+ tissues compared to N0 tissues (Figure 6J-K). Subsequently, we observed positive correlations between

An immunoprecipitation assay was performed using anti-Flag-LPL or anti-IgG (control) antibodies. The expression of ANGPTL4 and Furin was detected in the immunoprecipitants. (I-J) HGC27 cells transfected with Furin expression vector (I), ANGPTL4 expression vector (J), or control vector were treated with bafilomycin A1 (100 nmol/L) and increasing leptin for 8 h, and the alteration of LPL cleavage was detected by WB. (K) Expression of ANGPTL4 and Furin was detected in HGC27 cells that were stimulated with leptin for 4 h. (L) HGC27 cells were stimulated with leptin (200 ng/mL) or without leptin for 4 h. Immunofluorescent analysis was performed with anti-LPL and anti-ANGPTL4 antibodies. Scale bar, 20 μm. (M) WB analysis of LPL cleavage in leptin-treated HGC27 cells that were transfected with or without LEPR siRNA. Abbreviations: ANGPTL4, angiopoietin-like protein 4; ANGPTL4-oe, overexpression vector of ANGPTL4; FL, full-length; Furin-oe, overexpression vector of Furin; IB, immunoblotting; IGF-1, insulin like growth factor-1; IL-6, interleukin-6; LPL, lipoprotein lipase; N-ter, N-terminus; si-ANG, small interfering RNA of ANGPTL4; si-LEPR, small interfering RNA of LEPR; si-NC, negative control small interfering RNA; WB, western blotting.
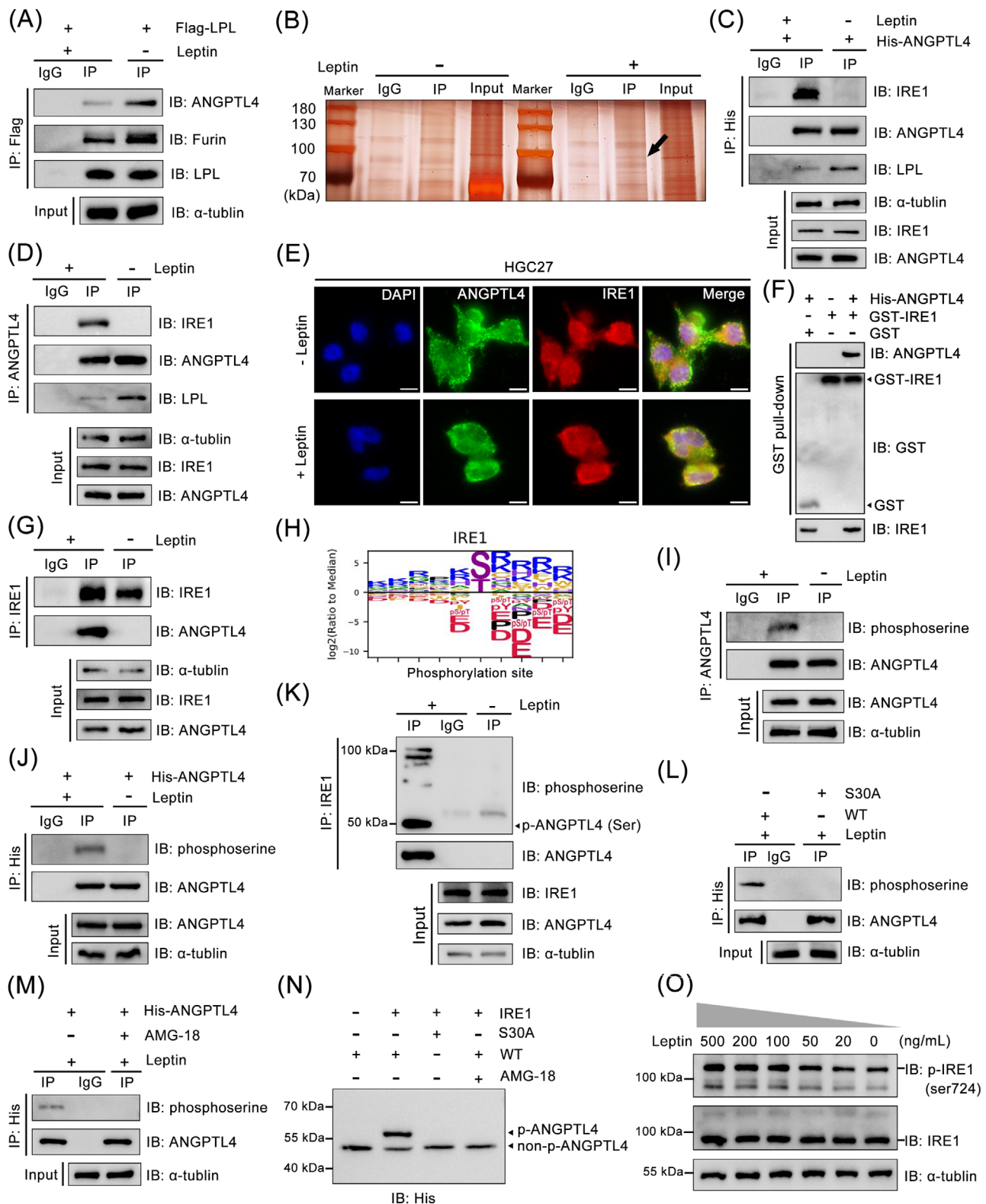
FIGURE 5 Leptin induced ANGPTL4 phosphorylation in an IRE1 kinase-dependent manner. (A) HGC27 cells expressing Flag-LPL were stimulated with leptin (200 ng/mL) or without leptin for 4 h. Protein lysates were immunoprecipitated with anti-Flag or anti-IgG (control) antibodies and analyzed by WB. (B) HGC27 cells with expression of His-ANGPTL4 were treated with leptin (200 ng/mL) or without leptin for 4 h. An immunoprecipitation assay was performed using an anti-His antibody, and immunoprecipitants were separated using SDS-PAGE and stained with silver. (C) HGC27 cells expressing His-ANGPTL4 were stimulated with leptin (200 ng/mL) or without leptin for 4 h. Cell lysates were analyzed by immunoprecipitation, followed by WB. (D) HGC27 cells were treated with leptin (200 ng/mL) or without leptin for 4 h. Protein lysates were then immunoprecipitated with anti-ANGPTL4 or anti-IgG (control) antibodies and analyzed by WB. (E)

the expression level of LEPR and both the circulating level of leptin ($r = 0.589$, $P < 0.001$) and the expression level of LPL ($r = 0.541$, $P < 0.001$) (Figure 6L-M). However, no significant difference was detected in ANGPTL4 expression between N0 and N+ tissues (Supplementary Figure S7E). Of note, leptin treatment enhanced intracellular lipid levels (Supplementary Figure S8A-B), and this effect could be mitigated by LEPR knockdown (Supplementary Figure S8C-D), AMG-18 administration (Supplementary Figure S8E-F), or LPL knockdown (Supplementary Figure S8G-H). Therefore, the activation of IRE1 by leptin and subsequent phosphorylation of ANGPTL4 contribute to the accumulation of lipids in GC cells.

3.8 | LPL activated the AA-COX2-PGE2-vascular endothelial growth factor C (VEGF-C) pathway in GC

To elucidate the role of LPL in gastric lipid homeostasis, we extracted total lipids from MKN45 cells with or without LPL knockdown for subsequent lipidomic analysis. Our findings, as depicted in Figure 7A, demonstrated that silencing LPL predominantly led to a reduction in glycerophospholipid levels, specifically phosphatidylcholine, phosphatidylinositol, and phosphatidylethanolamine. We subsequently performed GSEA based on the expression of LPL, utilizing RNA-seq data acquired from the Broad Institute Cancer Cell Line Encyclopedia (CCLE). The findings revealed significant enrichment of gene sets associated with LPL in glycerolipid metabolism, AA metabolism, and the epithelial-mesenchymal transition (EMT) pathway ($P < 0.050$) (Figure 7B). AA is derived directly from the diet or via the conversion of linoleic acid and normally exists in the form of esterified phospholipids within cell membranes [45]. Consequently, it could be

postulated that LPL may affect AA metabolism through modulation of the intracellular phospholipid composition or vice versa. After being transfected with LPL-targeting or control shRNA, GC cells were treated with VLDL or not. Following LPL knockdown, there was a noticeable reduction in the amount of AA in MKN45 cell lysates (Figure 7C). In footpad tumor tissue homogenates from HFD-fed mice, LPL knockdown also lowered the level of AA (Figure 7C). Correspondingly, ectopic expression of LPL significantly augmented AA accumulation in MKN45 cell lysates and footpad tumor tissue homogenates of mice fed on a CD (Supplementary Figure S9A). Prostanoids, such as prostaglandins (PGs) and thromboxane (TX), are the metabolites of AA. The conversion of AA into various prostanoids is conducted by the sequential actions of COXs and the respective prostanoid synthases [46]. Among the COX2-derived metabolites of AA, PGE2 is the most abundantly generated metabolite and has a prominent role in tumor LNM [47]. In line with this, the knockdown of LPL resulted in a decline in PGE2 abundances in both cell lysates and supernatants treated with VLDL, as well as in tissue samples from footpad tumors of mice fed on an HFD (Figure 7D; Supplementary Figure S9B). Conversely, overexpression of LPL promoted the accumulation of PGE2 in VLDL-treated GC cells and tissue homogenates of mice fed on a CD (Figure 7E; Supplementary Figure S9C). In effect, AA treatment led to an increase in PGE2 levels in the cell supernatants (Figure 7F; Supplementary Figure S9D); however, this effect was mitigated by silencing LPL (Figure 7G; Supplementary Figure S9E). Similarly, leptin also stimulated the secretion of PGE2, which was likewise suppressed by silencing LPL (Figure 7F and H; Supplementary Figure S9D and F). Tumor-associated lymphangiogenesis is primarily driven by VEGF-C, while PGE2 has been shown to promote VEGF-C expression in cancer [47]. To confirm this, MKN45 and HGC27 cells

---

Immunofluorescent analysis showing colocalization of IRE1 (red) and ANGPTL4 (green) in HGC27 cells treated with leptin. Nuclei were counterstained with DAPI (blue). Scale bar, 20 μm. (F) The purified His-tagged ANGPTL4 was incubated with either GST or GST-IRE1 coupled to glutathione-sepharose beads. The proteins retained on the sepharose were then subjected to immunoblotting using the indicated antibodies. (G) HGC27 cells were treated with leptin (200 ng/mL) or without leptin for 4 h. Protein lysates from HGC27 cells were then immunoprecipitated with an anti-IRE1 antibody and analyzed by WB. (H) Score site between IRE1 and ANGPTL4 as predicted by PhosphoSitePlus. (I-K) HGC27 cells were treated with leptin (200 ng/mL) or without leptin for 4 h. Then, using an antibody against phosphoserine, we evaluated phosphoserine expression in the immunoprecipitants from endogenous ANGPTL4 (I), exogenous His-ANGPTL4 (J), endogenous IRE1 (K), or IgG. (L) Parental HGC27 cells and the indicated clones of cells with expression of S30A-mutated ANGPTL4 (S30A) were both stimulated with leptin (200 ng/mL) for 4 h. Immunoprecipitation and WB analyses were performed as indicated. (M) HGC27 cells expressing His-ANGPTL4 were stimulated with leptin (200 ng/mL; 4 h) or AMG-18 (5 μmol/L; 4 h). The expression of phosphoserine in the immunoprecipitants was then detected by WB. (N) An In vitro kinase assay was performed in HGC27 cells by mixing purified wild-type His-ANGPTL4 (WT) or S30A-mutated His-ANGPTL4 (S30A) with or without active IRE1 in the presence of ATP. Then, the reaction mixture was separated by phos-tag SDS-PAGE and subjected to WB using an anti-His antibody. (O) Expression levels of p-IRE1 (ser724) and IRE1 in leptin-treated (200 ng/mL; 4 h) HGC27 cells. Abbreviations: ANGPTL4, angiopoietin-like protein 4; FL, full-length; IB, immunoblotting; IRE1, inositol-requiring enzyme 1; LPL, lipoprotein lipase; N-ter, N-terminus; S30A, serine 30 to alanine; SDS-PAGE, sodium dodecyl sulfate-polyacrylamide gel electrophoresis; WB, western blotting.
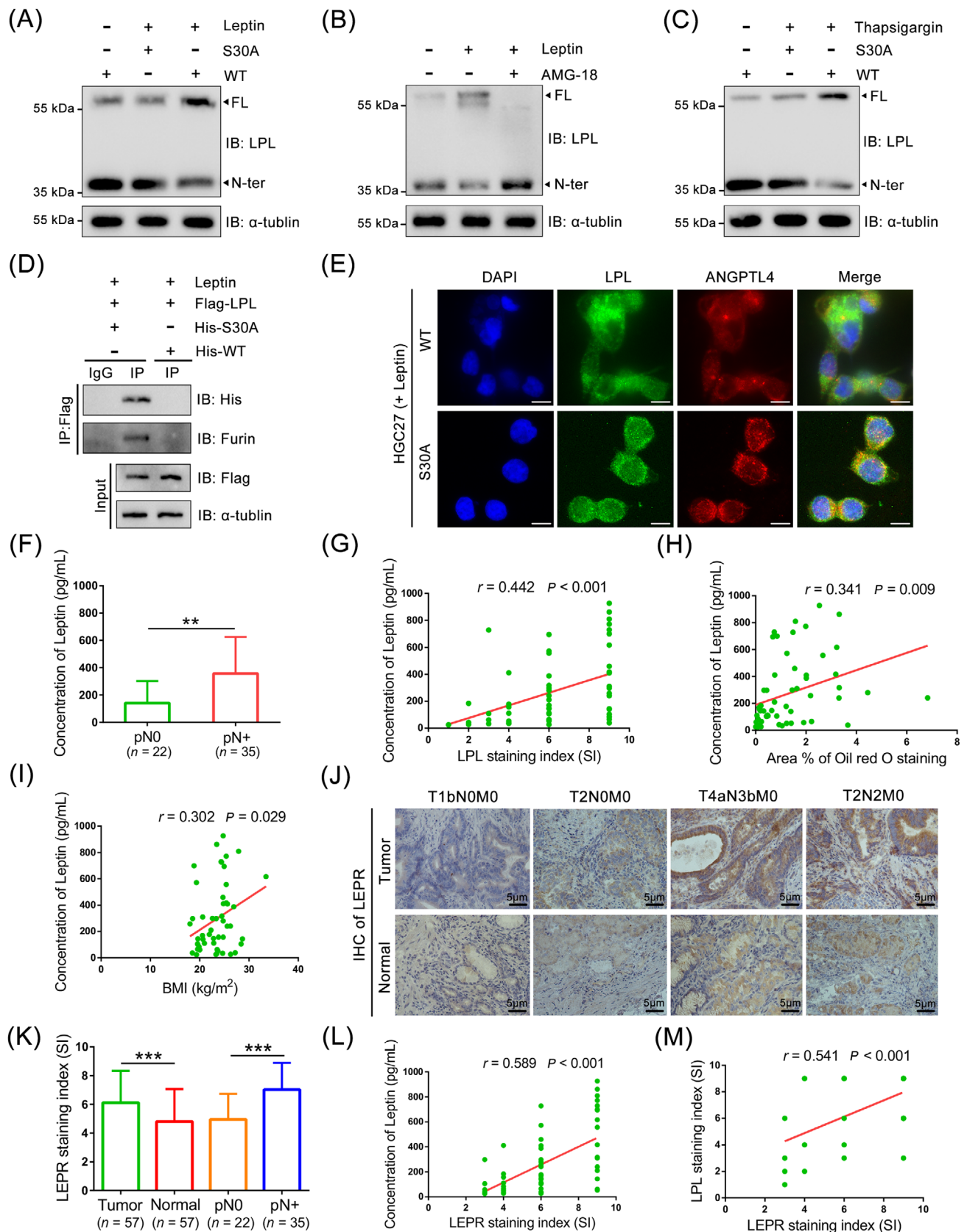
FIGURE 6 The signaling of leptin-LEPR-IRE1-ANGPTL4 suppressed LPL cleavage. (A) HGC27 cells expressing wild-type His-ANGPTL4 (WT) or S30A-mutated His-ANGPTL4 (S30A) were stimulated with leptin (200 ng/mL) or without leptin for 4 h. The expression of LPL was detected by WB. (B) WB analysis of LPL cleavage in HGC27 cells that were treated with leptin (200 ng/mL; 4 h) and/or AMG-18 (5 μmol/L; 4 h). (C) HGC27 cells expressing wild-type His-ANGPTL4 (WT) or S30A-mutated His-ANGPTL4 (S30A) were stimulated

were treated with increased levels of PGE2, resulting in elevated levels of VEGF-C and N-cadherin (a mesenchymal marker) as well as decreased expression of E-cadherin (an epithelial marker) in GC cell lysates (Figure 7I; Supplementary Figure S9G). Additionally, AA treatment also enhanced the expression of COX2 and VEGF-C in MKN45 cell lysates (Figure 7J). However, PGE2 or AA treatment did not affect LPL expression (Figure 7I-J; Supplementary Figure S9G). In VLDL-pretreated cells, the ectopic expression of LPL significantly enhanced the expression levels of COX2, VEGF-C, and N-cadherin, whereas the knockdown of endogenous LPL substantially suppressed their expression (Figure 7K). Meanwhile, LPL also inhibited the expression of E-cadherin (Figure 7K). As predicted, treatment with a COX2 inhibitor, celecoxib, or knockdown of COX2 effectively abolished the LPL-induced production of VEGF-C in VLDL-treated GC cells (Figure 7L-M; Supplementary Figure S9H-I). These results suggested that LPL elevated the abundance of AA in GC cells, thereby activating the AA-COX2-PGE2-VEGF-C pathway.

3.9 | Celecoxib blocked the role of LPL in LNM

To elucidate the role of PGE2 in LPL-mediated lymphangiogenesis, we utilized celecoxib or PGE2 to treat GC cells and collected corresponding CM. As illustrated in Figure 8A and Supplementary Figure S9J, celecoxib effectively counteracted the promoting effect of LPL or VLDL on the tube formation and migration of HLECs. Consistently, PGE2 significantly reversed the impact of LPL knockdown on HLEC tube formation and migration (Figure 8B; Supplementary Figure S9K). These findings were further substantiated by our in vivo experiments. Specifically, we separately introduced LPL-overexpressing MKN45 cells or control cells into the HFD mice and administered oral treatment with celecoxib to the designated group. Remarkably, celecoxib treatment signif-

icantly impeded the metastasis of LPL-overexpressing MKN45 cells to the popliteal LNs of nude mice (Figure 8C). Furthermore, celecoxib treatment significantly decreased the volume of popliteal LNs and the rate of LN metastasis compared to both control and LPL-overexpressing groups (Figure 8D-E). Notably, LPL overexpression led to an elevation in PGE2 levels in tissue homogenates obtained from primary footpad tumors; however, this effect was reversed by celecoxib (Figure 8F). Taken together, these findings strongly suggest that LPL promotes LNM of GC by stimulating the production of PGE2, and importantly, this effect can be effectively blocked by celecoxib (Figure 8G).

4 | DISCUSSION

Regardless of the high levels of de novo lipogenesis observed in cancer cells, the presence of LPL in tumor tissue highlights the significance of dietary lipid uptake [48]. The current study elucidated the crucial roles of LPL in gastric lipid deposition, particularly linking LPL-mediated dietary lipid uptake with LNM in GC. Furthermore, our study highlighted the interplay between LPL and AA metabolism. These results contributed to a deeper understanding of tumor prevention and management, particularly in relation to dietary interventions [48, 49]. Moreover, it offered novel insights into the diagnosis of LNM through assessing lipid levels or gene expression, as well as potential avenues for therapeutic intervention such as non-steroidal anti-inflammatory drugs (NSAIDs) or LPL inhibitors [50]. However, conducting a comprehensive analysis on how phosphorylation of ANGPTL4 impedes its binding with LPL, whether this phosphorylation affects ANGPTL4 secretion and cleavage [51], and how LPL facilitates AA production will aid in designing targeted interventions against this regulatory axis. In recent years, large-scale omics sequencing data combined with biological experiments have highlighted reprogramming of lipid metabolism in tumor cells; thus, targeting

---

with thapsigargin (600 nmol/L; 2 h) or without thapsigargin. The expression of LPL was detected by WB. (D) HGC27 cells were transduced with vectors expressing Flag-LPL, wild-type His-ANGPTL4 (His-WT), or S30A-mutated His-ANGPTL4 (His-S30A), and subsequently treated with leptin (200 ng/mL) for 4 h. Protein lysates were immunoprecipitated with anti-Flag or anti-IgG antibodies and analyzed by WB. (E) HGC27 cells expressing wild-type His-ANGPTL4 (WT) or S30A-mutated His-ANGPTL4 (S30A) were stimulated with leptin (200 ng/mL) for 4 h. The colocalization between LPL and ANGPTL4 was determined by immunofluorescence. Scale bar, 20 μm. (F) Circulating levels of leptin in the serum of 57 GC patients were detected by ELISA. (G-H) Pearson analyses between leptin levels and LPL expression (G), as well as the oil red O staining area (H) in 57 GC patients. (I) Correlation analyses between leptin level and BMI in 57 GC patients. (J-K) Representative images (J) and histogram analysis (K) of LEPR expression in 57 paired tumor tissues and adjacent normal tissues. Scale bar, 5 μm. (L) Correlation analyses between leptin level and LEPR expression in 57 GC patients. (M) Correlation analyses between LEPR expression and LPL expression in 57 GC patients. The data were presented as the mean ± SD. **$P < 0.01$; ***$P < 0.001$. Abbreviations: ANGPTL4, angiopoietin-like protein 4; BMI, body mass index; ELISA, enzyme-linked immunosorbent assay; FL, full-length; IB, immunoblotting; IP, immunoprecipitation; IRE1, inositol-requiring enzyme 1; LPL, lipoprotein lipase; N-ter, N-terminus; S30A, serine 30 to alanine; WB, western blotting.
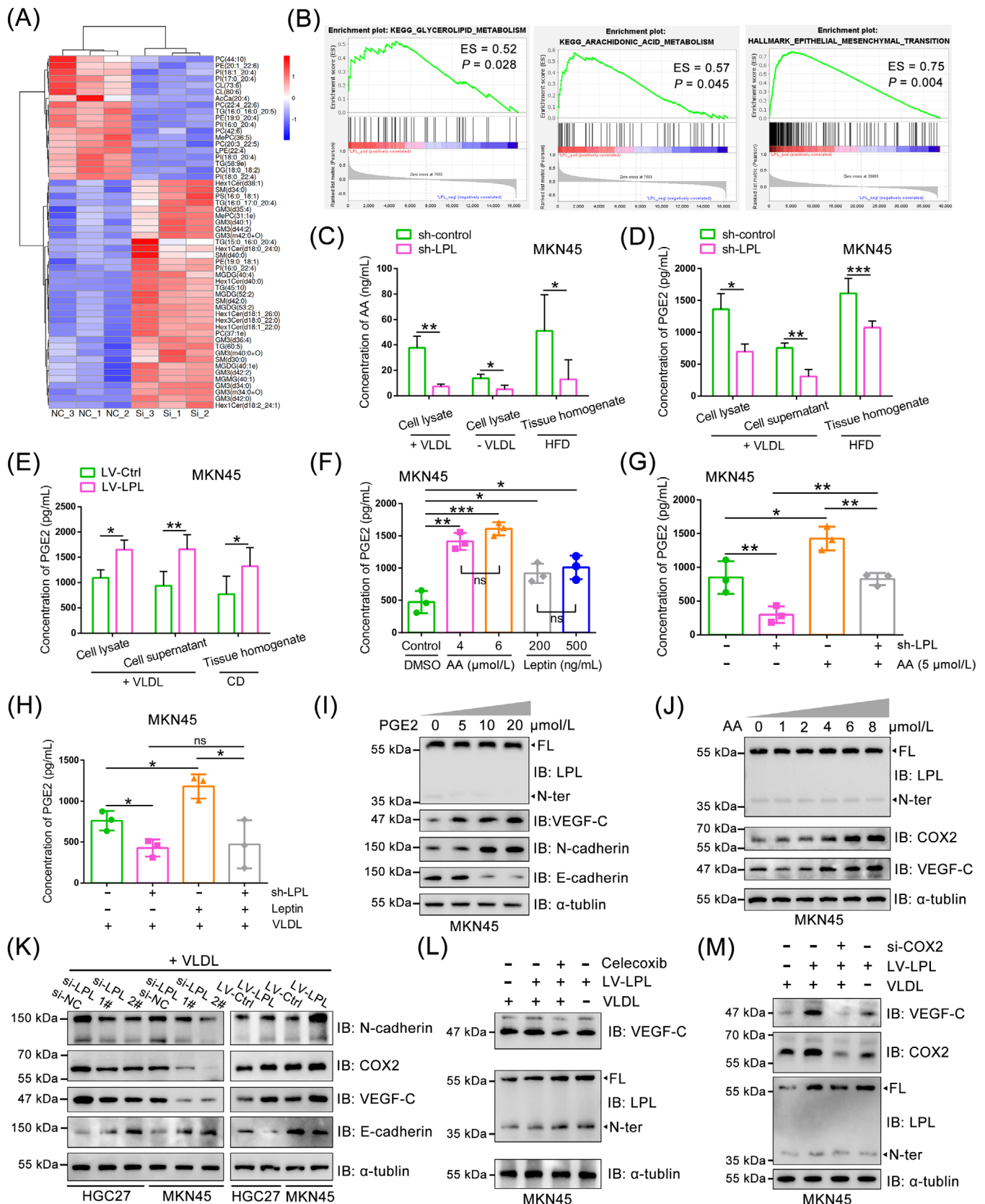
FIGURE 7 LPL activated the AA-COX2-PGE2-VEGF-C pathway in GC. (A) Heat map showing lipid metabolites identified by LC-MS in MKN45 cells transfected with or without LPL siRNA. (B) GSEA analysis of LPL by utilizing the RNA-seq data obtained from the CCLE database. (C) MKN45 cells transfected with LPL shRNA were treated with VLDL (25 μg/mL) or without VLDL for 24 h. Concentrations of AA in cell lysates, as well as footpad tumor tissue homogenates derived from HFD-fed mice, were determined by ELISA. (D) The levels of PGE2

lipid metabolism represents a promising strategy for future cancer treatment [52].

Of note, ANGPTL4 also undergoes proteolytic cleavage after secretion and is cleaved in a serum-dependent manner [51]. ANGPTL3, ANGPTL4, and ANGPTL8, all belonging to the family of angiopoietin-like proteins, are endogenous LPL antagonists and contribute to tissue-specific regulation of LPL [29]. ANGPTL8 functions as a molecular switch by forming complexes that activate ANGPTL3 while deactivating ANGPTL4 in their inhibition of LPL [53]. In other words, ANGPTL4 can directly affect the function of ANGPTL8 and indirectly participate in the regulation of ANGPTL3. Therefore, it is important to consider whether the phosphorylation of ANGPTL4 impacts the activities of ANGPTL3/8. However, these processes occur extracellularly or within the circulatory system, while our current study focuses on the intracellular regulatory relationship. Thus, it is crucial to investigate whether the phosphorylation of ANGPTL4 interferes with its own secretion and cleavage. In GC, Okochi-Takada *et al.* [54] reported that ANGPTL4 functions as a tumor suppressor that inhibits angiogenesis, whereas some studies [55, 56] have suggested its association with GC venous invasion and promotion of GC cell migration and invasion. In our study, no significant difference in ANGPTL4 expression was observed; however, the phosphorylation of ANGPTL4 resulted in a loss of function for ANGPTL4, leading to inhibited LPL cleavage and enhanced lipid accumulation. The inconsistency between these studies may arise from differences in cell treatment or the cleavage of ANGPTL4 [57]. In this context, it reminds us that additional studies are needed to confirm the specific role of ANGPTL4 in GC, in particular, the phosphorylated ANGPTL4.

Leptin affects lipid metabolism independently of its well-known effects on feeding and energy expenditure, but exactly how this occurs is ill-defined [58]. Specifically, the regulation of LPL activity by leptin has already been identified in hepatocytes [58], macrophages [59], and severely obese patients [38], while our work uncovered a novel mechanism by which leptin modulates LPL by inhibiting ANGPTL4-mediated LPL cleavage in an IRE1-dependent manner. IRE1 serves as a crucial sensor for ER stress, including protein folding stress triggered by an accumulation of unfolded proteins in the ER lumen and ER membrane lipid bilayer stress induced by an accumulation of cholesterol or saturated fatty acids [44]. Since we found that thapsigargin (an inhibitor of the ER Ca^{2+} pump) can also initiate the phosphorylation of ANGPTL4, it is imperative to investigate whether the activation of IRE1 stems from leptin-induced ER stress or alternative pathways.

Recent epidemiological studies and clinical trials have provided compelling evidence that long-term use of aspirin and other NSAIDs can significantly reduce the incidence of some malignancies [60]. Notably, NSAIDs primarily exert their effects by targeting cyclooxygenase enzymes responsible for converting AA into PGs and TX [60]. COX2-derived PGE2, upon binding to its receptors, can activate signaling pathways involved in regulating lymphangiogenesis [47]. Our study also unveiled the pivotal role of PGE2 in promoting GC lymphangiogenesis and further substantiated the inhibitory effect of celecoxib on the LNM of GC, thereby underscoring the potential therapeutic value of COX2 inhibitors in GC treatment.

Although the present study demonstrated that LPL-mediated lipid uptake could enhance LNM in GC, further analysis is warranted to determine whether this effect also contributes to other modes of metastasis in GC, such as hematogenous metastasis and peritoneal metastasis. This will help ascertain whether lipid accumulation is a distinctive characteristic of LNM in GC. Additionally, larger sample sizes are necessary to validate the differences in lipid accumulation and LPL expression between N+ and N0 samples. Furthermore, it is essential to prospectively assess the predictive value of these indicators for LNM by

---

were measured using ELISA in VLDL-treated MKN45 cells and primary footpad tumors of mice fed an HFD. (E) MKN45 cells transfected with LPL-overexpressing vector were treated with VLDL (25 μg/mL) for 24 h. Concentrations of PGE2 in cell lysates, cell supernatants, and primary footpad tumors of mice fed a CD, were determined by ELISA. (F) The concentration of PGE2 in the supernatants of MKN45 cells treated with AA (48 h), leptin (24 h), and DMSO (control) was measured by ELISA. (G) MKN45 cells transduced with LPL shRNA or control shRNA were exposed to AA (5 μmol/L) or not for 48 h, and the concentration of PGE2 in the cell supernatants was determined using ELISA. (H) MKN45 cells transduced with LPL shRNA or control shRNA were treated with VLDL (25 μg/mL; 24 h) and stimulated with leptin (200 ng/mL; 24 h) or without leptin. The concentration of PGE2 in the cell supernatants was assessed by ELISA. (I-J) WB analysis was performed on MKN45 cells that were exposed to increasing concentrations of PGE2 (I) or AA (J) for 48 h. (K) WB analysis of VLDL-treated GC cells transfected with LPL siRNA, LPL vector, control siRNA, or control empty vector. (L) MKN45 cells overexpressing LPL were treated with VLDL (25 μg/mL; 48 h) and/or celecoxib (25 μmol/L; 48 h) as indicated, and protein expression was detected by WB. (M) MKN45 cells expressing LPL were treated with VLDL (25 μg/mL; 48 h) and/or COX2 siRNA (25 nmol/L; 48 h) as indicated, and protein expression was detected by WB. The data were presented as the mean ± SD. The *P* value was calculated by paired t test. *P < 0.05, **P < 0.01, ***P < 0.001, ns, not significant. Abbreviations: AA, arachidonic acid; CD, control diet; COX2, cyclooxygenase-2; ELISA, enzyme-linked immunosorbent assay; ES, enrichment score; FL, full-length; HFD, high-fat diet; IB, immunoblotting; LPL, lipoprotein lipase; N-ter, N-terminus; PGE2, prostaglandin E2; SD, standard deviation; VEGF-C, vascular endothelial growth factor C; VLDL, very low-density lipoproteins; WB, western blotting.
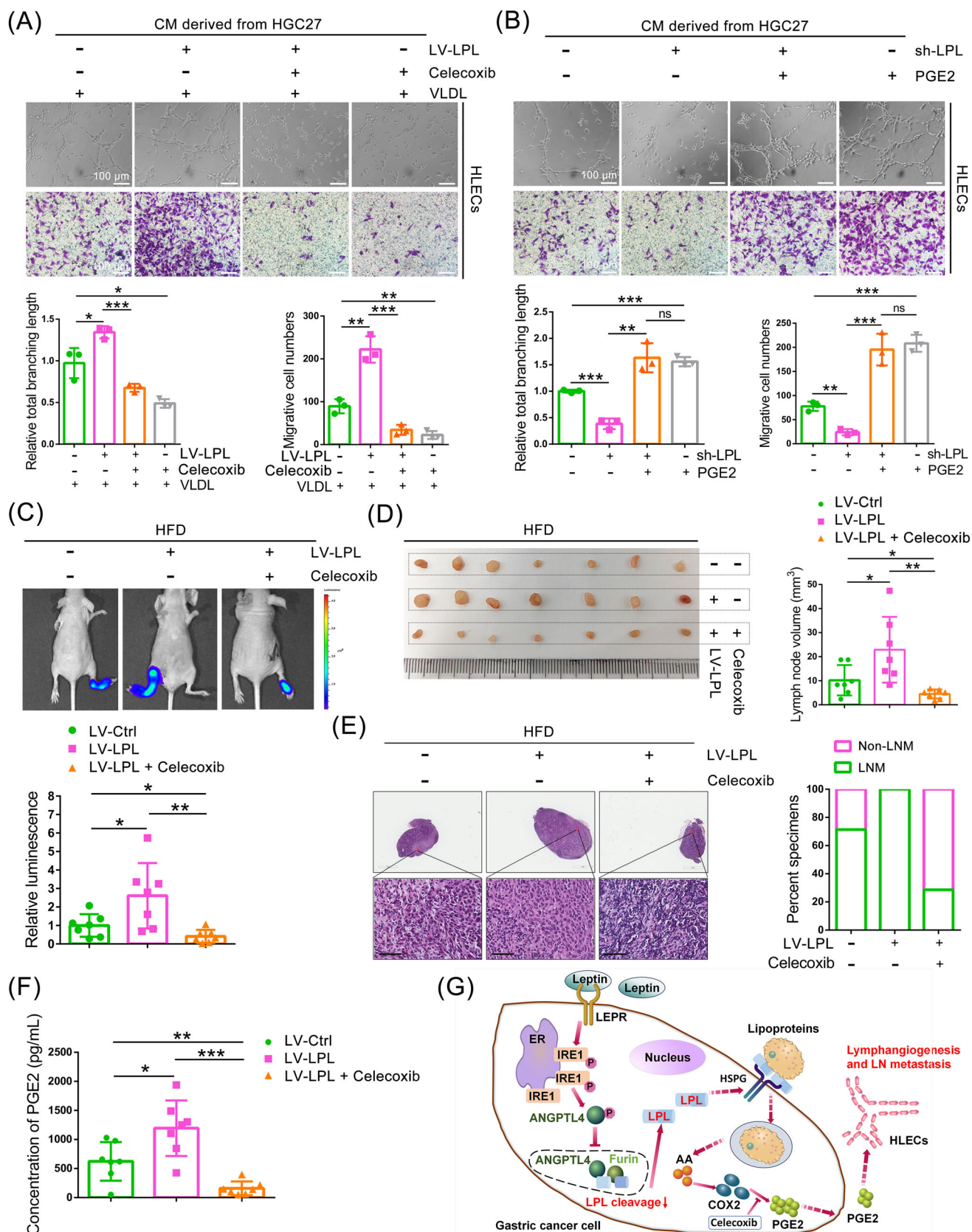
FIGURE 8 Celecoxib blocked the role of LPL in LNM. (A) HGC27 cells were treated with VLDL (25 μg/mL), LPL-overexpressing vectors, or celecoxib (25 μmol/L). Representative images (upper panel) and quantification (lower panel) of the tube formation and transwell migration of HLECs cocultured with CM derived from indicated HGC27 cells were shown. Scale bar, 100 μm. (B) HGC27 cells were treated with LPL-targeting shRNA and/or PGE2 (10 μmol/L). Representative images (upper panel) and quantification (lower panel) of the tube formation

and transwell migration of HLECs cocultured with CM derived from indicated HGC27 cells were shown. Scale bar, 100 μm. (C) HFD-fed mice were injected with LPL-overexpressing MKN45 cells or control cells in the footpad, and mice were then either treated with celecoxib or not. Representative images of bioluminescence (upper panel) and histogram analysis (lower panel) of popliteal LNM in the indicated mouse groups were shown ($n = 7$ per group). (D) Representative images of the enucleated popliteal LNs (left panel) mentioned in (C) and histogram analysis of the LN volume (right panel; $n = 7$ per group). (E) Representative images (left panel) and histogram analysis of popliteal LN status (right panel). Scale bar for H&E staining was 1 mm (upper panel) or 60 μm (lower panel). (F) The concentration of PGE2 in tissue homogenates from primary footpad tumors mentioned in (C) was assessed by ELISA. (G) A schematic model of the mechanism underlying the role of LPL in LNM. Leptin binding with LEPR could induce IRE1 kinase to phosphorylate ANGPTL4 at the Ser30 residue, thereby inhibiting the binding of ANGPLT4 to LPL and blocking the cleavage of LPL by ANGPTL4/Furin, thus upregulating the expression of LPL in GC cells. The upregulation of LPL then increased the level of AA in GC cells, triggered the COX2/PGE2 pathway, and enhanced the expression of VEGF-C, thus promoting lymphangiogenesis and LNM in GC. The data were presented as the mean ± SD. The P value was calculated by paired t test. *$P < 0.05$, **$P < 0.01$, ***$P < 0.001$, ns, not significant. Abbreviations: AA, arachidonic acid; ANGPTL4, angiopoietin-like protein 4; CM, conditional medium; COX2, cyclooxygenase-2; ELISA, enzyme-linked immunosorbent assay; ER, endoplasmic reticulum; HSPG, heparan sulfate proteoglycan; IRE1, inositol-requiring enzyme 1; LEPR, leptin receptor; LNM, lymph node metastasis; LPL, lipoprotein lipase; PGE2, prostaglandin E2; VEGF-C, vascular endothelial growth factor C; VLDL, very low-density lipoproteins.

examining preoperative gastroscopy tissues. Lastly, additional analysis is needed to elucidate how LPL influences glycerophospholipid metabolism in GC cells.

5 | CONCLUSIONS

In summary, our study revealed that leptin binding to LEPR induces IRE1 to phosphorylate ANGPTL4 and thus inhibits ANGPTL4/Furin-mediated LPL cleavage. The upregulated expression of LPL then contributes to the exogenous lipid supply and activates the AA-COX2-PGE2-VEGF-C pathway to promote LNM in GC.

AUTHOR CONTRIBUTIONS

Jian Xiao and Li Yang: Designed the experiments. **Jian Xiao, Suqing Cao, Pengyu Li, and Jiawei Wang**: Performed the animal, functional, and biochemical experiments. **Quan Cheng**: Performed bioinformatical analyses and IHC staining. **Xinyi Zhou and Jiacheng Dong**: Performed some animal and biochemical experiments. **Yuan Li and Xinyu Zhao**: Assisted in the analysis of some experiments and interpreted the data. **Jian Xiao**: Drafted the manuscript. **Zekuan Xu and Li Yang**: Conceived and supervised the project. All authors have reviewed and approved the submission.

CONFLICT OF INTEREST STATEMENT

The authors declare no competing interests.

DATA AVAILABILITY STATEMENT

All the data is present in the manuscript and the supplementary materials. Additional data related to this paper may be requested from the corresponding author. The original WB was uploaded as supplementary materials.

ETHICS APPROVAL AND CONSENT TO PARTICIPATE

The specimens of patients with gastric cancer were collected with permission from the Ethics Committee of the First Affiliated Hospital of Nanjing Medical University (permit number: 2022-SR-597). The tissue samples were obtained with written informed consent from each patient. All animal experiments were conducted according to animal protocols approved by Nanjing Medical University and were approved by the Ethics Committee of Nanjing Medical University (permit number: IACUC-2203027).

ORCID

Li Yang https://orcid.org/0000-0001-5456-1944

REFERENCES

1. Sung H, Ferlay J, Siegel RL, Laversanne M, Soerjomataram I, Jemal A, et al. Global Cancer Statistics 2020: GLOBOCAN Estimates of Incidence and Mortality Worldwide for 36 Cancers in 185 Countries. CA Cancer J Clin. 2021;71(3):209–249.
2. Zheng R, Zhang S, Zeng H, Wang S, Sun K, Chen R, et al. Cancer incidence and mortality in China, 2016. J Natl Cancer Cent. 2022;2(1):1–9.
3. Feng R, Su Q, Huang X, Basnet T, Xu X, Ye W. Cancer situation in China: what does the China cancer map indicate from the first national death survey to the latest cancer registration? Cancer Commun (Lond). 2023;43(1):75–86.

4. Wang Z, Han W, Xue F, Zhao Y, Wu P, Chen Y, et al. Nationwide gastric cancer prevention in China, 2021-2035: a decision analysis on effect, affordability and cost-effectiveness optimisation. Gut. 2022;71(12):2391–2400.

5. Japanese gastric cancer treatment guidelines 2018 (5th edition). Gastric Cancer. 2021;24(1):1–21.

6. Reticker-Flynn NE, Zhang W, Belk JA, Basto PA, Escalante NK, Pilarowski GOW, et al. Lymph node colonization induces tumor-immune tolerance to promote distant metastasis. Cell. 2022;185(11):1924–1942.e23.

7. Joshi SS, Badgwell BD. Current treatment and recent progress in gastric cancer. CA Cancer J Clin. 2021;71(3):264–279.

8. Ricci AD, Rizzo A, Brandi G. DNA damage response alterations in gastric cancer: knocking down a new wall. Future Oncol. 2021;17(8):865–868.

9. Ricci AD, Rizzo A, Rojas Llimpe FL, Di Fabio F, De Biase D, Rihawi K. Novel HER2-Directed Treatments in Advanced Gastric Carcinoma: AnotHER Paradigm Shift? Cancers (Basel). 2021;13(7):1664.

10. Santoni M, Rizzo A, Mollica V, Matrana MR, Rosellini M, Faloppi L, et al. The impact of gender on The efficacy of immune checkpoint inhibitors in cancer patients: The MOUSEION-01 study. Crit Rev Oncol Hematol. 2022;170:103596.

11. Bian X, Liu R, Meng Y, Xing D, Xu D, Lu Z. Lipid metabolism and cancer. J Exp Med. 2021;218(1):e20201606.

12. Martin-Perez M, Urdiroz-Urricelqui U, Bigas C, Benitah SA. The role of lipids in cancer progression and metastasis. Cell Metab. 2022;34(11):1675–1699.

13. Dai W, Xiang W, Han L, Yuan Z, Wang R, Ma Y, et al. PTPRO represses colorectal cancer tumorigenesis and progression by reprogramming fatty acid metabolism. Cancer Commun (Lond). 2022;42(9):848–867.

14. Lee CK, Jeong SH, Jang C, Bae H, Kim YH, Park I, et al. Tumor metastasis to lymph nodes requires YAP-dependent metabolic adaptation. Science. 2019;363(6427):644–649.

15. Majima M, Hosono K, Ito Y, Amano H. Biologically active lipids in the regulation of lymphangiogenesis in disease states. Pharmacol Ther. 2022;232:108011.

16. Ogawa F, Amano H, Eshima K, Ito Y, Matsui Y, Hosono K, et al. Prostanoid induces premetastatic niche in regional lymph nodes. J Clin Invest. 2014;124(11):4882–4894.

17. Xiao J, Shen K, Liu K, Wang Y, Fan H, Cheng Q, et al. Obesity promotes lipid accumulation in lymph node metastasis of gastric cancer: a retrospective case–control study. Lipids Health Dis. 2022;21(1):123.

18. Zaidi N, Lupien L, Kuemmerle NB, Kinlaw WB, Swinnen JV, Smans K. Lipogenesis and lipolysis: the pathways exploited by the cancer cells to acquire fatty acids. Prog Lipid Res. 2013;52(4):585–589.

19. Corn KC, Windham MA, Rafat M. Lipids in the tumor microenvironment: From cancer progression to treatment. Prog Lipid Res. 2020;80:101055.

20. Mahmud I, Tian G, Wang J, Hutchinson TE, Kim BJ, Awasthee N, et al. DAXX drives de novo lipogenesis and contributes to tumorigenesis. Nat Commun. 2023;14(1):1927.

21. Li S, Wu T, Lu YX, Wang JX, Yu FH, Yang MZ, et al. Obesity promotes gastric cancer metastasis via diacylglycerol acyltransferase 2-dependent lipid droplets accumulation and redox homeostasis. Redox Biol. 2020;36:101596.

22. Jiang M, Wu N, Xu B, Chu Y, Li X, Su S, et al. Fatty acid-induced CD36 expression via O-GlcNAcylation drives gastric cancer metastasis. Theranostics. 2019;9(18):5359–5373.

23. Kitayama J, Hatano K, Kaisaki S, Suzuki H, Fujii S, Nagawa H. Hyperlipidaemia is positively correlated with lymph node metastasis in men with early gastric cancer. Br J Surg. 2004;91(2):191–198.

24. Kim H, Song Z, Zhang R, Davies BSJ, Zhang K. A hepatokine derived from the ER protein CREBH promotes triglyceride metabolism by stimulating lipoprotein lipase activity. Sci Signal. 2023;16(768):eadd6702.

25. Olivecrona G. Role of lipoprotein lipase in lipid metabolism. Curr Opin Lipidol. 2016;27(3):233–241.

26. Lupien LE, Bloch K, Dehairs J, Traphagen NA, Feng WW, Davis WL, et al. Endocytosis of very low-density lipoproteins: an unexpected mechanism for lipid acquisition by breast cancer cells. J Lipid Res. 2020;61(2):205–218.

27. Wu Z, Ma H, Wang L, Song X, Zhang J, Liu W, et al. Tumor suppressor ZHX2 inhibits NAFLD-HCC progression via blocking LPL-mediated lipid uptake. Cell Death Differ. 2020;27(5):1693–1708.

28. Kuemmerle NB, Rysman E, Lombardo PS, Flanagan AJ, Lipe BC, Wells WA, et al. Lipoprotein lipase links dietary fat to solid tumor cell proliferation. Mol Cancer Ther. 2011;10(3):427–436.

29. Wu SA, Kersten S, Qi L. Lipoprotein Lipase and Its Regulators: An Unfolding Story. Trends Endocrinol Metab. 2021;32(1):48–61.

30. Xiao J, Lin L, Luo D, Shi L, Chen W, Fan H, et al. Long noncoding RNA TRPM2-AS acts as a microRNA sponge of miR-612 to promote gastric cancer progression and radioresistance. Oncogenesis. 2020;9(3):29.

31. Aoki T, Kinoshita J, Munesue S, Hamabe-Horiike T, Yamaguchi T, Nakamura Y, et al. Hypoxia-Induced CD36 Expression in Gastric Cancer Cells Promotes Peritoneal Metastasis via Fatty Acid Uptake. Ann Surg Oncol. 2023;30(5):3125–3136.

32. Cheng Q, Liu K, Xiao J, Shen K, Wang Y, Zhou X, et al. SEC23A confers ER stress resistance in gastric cancer by forming the ER stress-SEC23A-autophagy negative feedback loop. J Exp Clin Cancer Res. 2023;42(1):232.

33. Ma X, Wang G, Fan H, Li Z, Chen W, Xiao J, et al. Long noncoding RNA FAM225A promotes the malignant progression of gastric cancer through the miR-326/PADI2 axis. Cell Death Discov. 2022;8(1):20.

34. Győrffy B. Transcriptome-level discovery of survival-associated biomarkers and therapy targets in non-small-cell lung cancer. Br J Pharmacol. 2024;181(3):362–374.

35. Jin N, Matter WF, Michael LF, Qian Y, Gheyi T, Cano L, et al. The Angiopoietin-Like Protein 3 and 8 Complex Interacts with Lipoprotein Lipase and Induces LPL Cleavage. ACS Chem Biol. 2021;16(3):457–462.

36. Dijk W, Ruppert PMM, Oost LJ, Kersten S. Angiopoietin-like 4 promotes the intracellular cleavage of lipoprotein lipase by PCSK3/furin in adipocytes. J Biol Chem. 2018;293(36):14134–14145.

37. Karaman S, Detmar M. Mechanisms of lymphatic metastasis. J Clin Invest. 2014;124(3):922–928.

38. Ramis JM, Bibiloni B, Moreiro J, García-Sanz JM, Salinas R, Proenza AM, et al. Tissue leptin and plasma insulin are associated with lipoprotein lipase activity in severely obese patients. J Nutr Biochem. 2005;16(5):279–285.

39. Hopkins BD, Goncalves MD, Cantley LC. Obesity and Cancer Mechanisms: Cancer Metabolism. J Clin Oncol. 2016;34(35):4277–4283.

40. Masuno H, Sakayama K, Okuda H. Effect of long-term treatment of 3T3-L1 adipocytes with chlorate on the synthesis, glycosylation, intracellular transport and secretion of lipoprotein lipase. Biochem J. 1998;329(Pt 3):461–468.

41. de Candia P, Prattichizzo F, Garavelli S, Alviggi C, La Cava A, Matarese G. The pleiotropic roles of leptin in metabolism, immunity, and cancer. J Exp Med. 2021;218(5):e20191593.

42. Chen Y, Brandizzi F. IRE1: ER stress sensor and cell fate executor. Trends Cell Biol. 2013;23(11):547–555.

43. Hornbeck PV, Zhang B, Murray B, Kornhauser JM, Latham V, Skrzypek E. PhosphoSitePlus, 2014: mutations, PTMs and recalibrations. Nucleic Acids Res. 2015;43(Database issue):D512–D520.

44. Yildirim Z, Baboo S, Hamid SM, Dogan AE, Tufanli O, Robichaud S, et al. Intercepting IRE1 kinase-FMRP signaling prevents atherosclerosis progression. EMBO Mol Med. 2022;14(4):e15344.

45. Korbecki J, Rębacz-Maron E, Kupnicka P, Chlubek D, Baranowska-Bosiacka I. Synthesis and Significance of Arachidonic Acid, a Substrate for Cyclooxygenases, Lipoxygenases, and Cytochrome P450 Pathways in the Tumorigenesis of Glioblastoma Multiforme, Including a Pan-Cancer Comparative Analysis. Cancers (Basel). 2023;15(3):946.

46. Stack E, DuBois RN. Regulation of cyclo-oxygenase-2. Best Pract Res Clin Gastroenterol. 2001;15(5):787–800.

47. Lala PK, Nandi P, Majumder M. Roles of prostaglandins in tumor-associated lymphangiogenesis with special reference to breast cancer. Cancer Metastasis Rev. 2018;37(2-3):369–384.

48. Butler LM, Perone Y, Dehairs J, Lupien LE, de Laat V, Talebi A, et al. Lipids and cancer: Emerging roles in pathogenesis, diagnosis and therapeutic intervention. Adv Drug Deliv Rev. 2020;159:245–293.

49. Martínez-Garay C, Djouder N. Dietary interventions and precision nutrition in cancer therapy. Trends Mol Med. 2023;29(7):489–511.

50. Hao X, Zhu X, Tian H, Lai G, Zhang W, Zhou H, et al. Pharmacological effect and mechanism of orlistat in anti-tumor therapy: A review. Medicine (Baltimore). 2023;102(36):e34671.

51. Zuo Y, He Z, Chen Y, Dai L. Dual role of ANGPTL4 in inflammation. Inflamm Res. 2023;72(6):1303–1313.

52. Cheng C, Geng F, Cheng X, Guo D. Lipid metabolism reprogramming and its potential targets in cancer. Cancer Commun (Lond). 2018;38(1):27.

53. Zhang R, Zhang K. A unified model for regulating lipoprotein lipase activity. Trends Endocrinol Metab. 2024;23:S1043–2760(24)00045–6.

54. Okochi-Takada E, Hattori N, Tsukamoto T, Miyamoto K, Ando T, Ito S, et al. ANGPTL4 is a secreted tumor suppressor that inhibits angiogenesis. Oncogene. 2014;33(17):2273–2278.

55. Nakayama T, Hirakawa H, Shibata K, Abe K, Nagayasu T, Taguchi T. Expression of angiopoietin-like 4 in human gastric cancer: ANGPTL4 promotes venous invasion. Oncol Rep. 2010;24(3):599–606.

56. Chen JW, Luo YJ, Yang ZF, Wen LQ, Huang L. Knockdown of angiopoietin-like 4 inhibits the development of human gastric cancer. Oncol Rep. 2018;39(4):1739–1746.

57. Hübers C, Abdul Pari AA, Grieshober D, Petkov M, Schmidt A, Messmer T, et al. Primary tumor-derived systemic nANGPTL4 inhibits metastasis. J Exp Med. 2023;220(1):e20202595.

58. Huynh FK, Neumann UH, Wang Y, Rodrigues B, Kieffer TJ, Covey SD. A role for hepatic leptin signaling in lipid metabolism via altered very low density lipoprotein composition and liver lipase activity in mice. Hepatology. 2013;57(2):543–554.

59. Maingrette F, Renier G. Leptin increases lipoprotein lipase secretion by macrophages: involvement of oxidative stress and protein kinase C. Diabetes. 2003;52(8):2121–2128.

60. Wang D, Dubois RN. Prostaglandins and cancer. Gut. 2006;55(1):115–122.

SUPPORTING INFORMATION

Additional supporting information can be found online in the Supporting Information section at the end of this article.